The WalKR two-component regulator coordinates cell wall homeostasis with DNA replication in *Staphylococcus aureus*

Liam K. R. Sharkey[1], Romain Guerillot[1], Calum J. Walsh[1], Adrianna M. Turner[1], Jean Y. H. Lee[1], Stephanie L. Neville[1], Stephan Klatt[2], Sarah L. Baines[1], Sacha J. Pidot[1], Fernando J. Rossello[3,4], Torsten Seemann[1,5], Hamish E. G. McWilliam[1], Ellie Cho[6], Benjamin P. Howden[1,5], Christopher A. McDevitt[1], Abderrahman Hachani[1], Timothy P. Stinear[1,5,*] and Ian R. Monk[1,*]

1. Department of Microbiology and Immunology, Doherty Institute for Infection and Immunity, University of Melbourne, Melbourne, Victoria, 3000, Australia
2. The Florey Institute of Neuroscience and Mental Health, Melbourne Dementia Research Centre, The University of Melbourne, Parkville, Victoria, 3010, Australia.
3. University of Melbourne Centre for Cancer Research, The University of Melbourne, Melbourne, Victoria, 3000, Australia.
4. Australian Regenerative Medicine Institute, Monash University, Melbourne, Victoria, 3800, Australia.
5. Centre for Pathogen Genomics, Department of Microbiology and Immunology, Doherty Institute for Infection and Immunity, University of Melbourne, Melbourne, Victoria, 3000, Australia
6. Biological Optical Microscopy Platform, University of Melbourne, Melbourne, Victoria, 3000, Australia

* Joint senior authors

Keywords: Staphylococcus aureus, regulation, gene expression, two-component regulator, essential gene, WalKR

Abstract

Among the 16 two-component systems (TCSs) in the opportunistic human pathogen *Staphylococcus aureus*, only WalKR is essential. Like orthologous systems in other Bacillota, *S. aureus* WalKR controls autolysins involved in peptidoglycan remodelling and is therefore intimately involved in cell division. However, despite the importance of WalKR in *S. aureus*, the basis for its essentiality is not understood and the regulon poorly defined. Here, we use a panel of isogenic *walKR* mutants with a spectrum of activity, combined with functional genomics including ChIP-seq to identify a consensus WalR DNA-binding motif and define the direct WalKR regulon. As previously shown, the direct regulon includes multiple autolysin genes. However, we also show WalR directly regulates at least five essential genes involved in (i) lipoteichoic acid synthesis (*ltaS*), (ii) translation *(rplK*)*,* (iii) DNA compaction (*hup*), (iv) initiation of DNA replication (*dnaA, hup*) and (v) purine nucleotide metabolism (*prs*). Thus, WalKR in *S. aureus* is a polyfunctional regulator with fundamental control over critical cell systems, linking cell wall homeostasis with purine biosynthesis, protein biosynthesis, and DNA replication. Our findings explain the essentiality of this locus and should reignite interest in WalKR as a *bona fide* target for novel anti-staphylococcal therapeutics.

43 ## Introduction

44 *Staphylococcus aureus* is an opportunistic pathogen that causes a wide range of hospital and
45 community acquired infections. Antibiotic-resistant strains (in particular methicillin resistant
46 [MRSA] and vancomycin-intermediate [VISA] strains) are persistent problems, with last-line
47 agents, such as vancomycin, linezolid, and daptomycin, commonly failing [1, 2]. MRSA is a World
48 Health Organisation "priority antibiotic-resistant pathogen" for the research and
49 development of new antibiotics. In industrialised countries, *S. aureus* is responsible for an
50 annual bacteraemia rate of 10-30 cases/100,000 individuals per year, as well as high rates of
51 endocarditis, osteomyelitis, and skin and soft tissue infections [3]. Mortality from serious
52 *S. aureus* infection is high (20 - 50% of bacteraemias) [4], and the socioeconomic burden of
53 *S. aureus* disease is significant [5].

54 *S. aureus* encodes 16 core genome two-component systems (TCSs) which allow it to
55 sense and respond to a range of stimuli, providing regulatory flexibility in changeable
56 environments. Of these 16 TCSs, only WalKR is essential for cell viability under laboratory
57 conditions [6, 7, 8, 9]. WalKR is a canonical TCS that is conserved amongst low-GC Gram-positive
58 bacteria. It is composed of a multi-domain transmembrane sensor histidine kinase (WalK) and
59 DNA binding response regulator (WalR) of the OmpR family [10, 11]. Upon activation by an
60 extracellular signal WalK auto-phosphorylates a conserved histidine residue (H385) and
61 subsequently transfers the phosphoryl group to a conserved aspartate residue on WalR (D53).
62 Phosphorylated WalR binds to promoter regions of genes within the WalKR regulon,
63 operating as either a transcriptional activator or repressor.

64 WalKR is a master regulator of cell-wall homeostasis through the control of a suite of
65 autolysins [8, 12, 13, 14]. Although the locus is highly conserved, several points of difference
66 between bacterial genera suggest variation in the precise cellular function of the system and
67 resultant mechanism(s) of the essentiality. WalKR is within an operon of 3-6 genes that also
68 includes varying numbers of accessory factors. The operon can be classified into three
69 structures; bacilli and listeria have a six-gene operon (*walR*, *walK*, *yycH*, *yycI*, *yycJ*, *yycK*),
70 whereas staphylococci, lactobacilli and enterococci lack the final gene *yycK* (a serine protease)
71 [15], with only three genes present in streptococci; *walR, walK,* and *yycJ* [16]. Two accessory
72 genes, *yycH* and *yycI* encode membrane associated proteins that differ in their function across
73 genera; in *S. aureus* these proteins are activators of WalKR activity whereas in *Bacillus subtilis*
74 they function as repressors [17, 18]. A second key difference between the systems is how WalKR
75 interacts with the division septum. In *B. subtilis*, WalK controls the expression of FtsZ [19], it is
76 localised to the division septum in an FtsZ dependent manner and interacts with proteins of
77 the divisome. Consequently, WalKR essentiality in *B. subtilis* arises from the co-ordination of
78 cell wall remodelling with cell division, in response to signalling via an extracellular PAS
79 domain [16, 20, 21, 22]. In *S. aureus*, WalK is also reported to localise to the division septum in
80 growing cells [23]. However, there is no evidence of interaction with proteins of the divisome
81 and FtsZ has not been mapped to the staphylococcal WalKR regulon. In *Streptococcus*
82 *pneumoniae*, WalKR essentiality can be attributed to the regulation of a single gene encoding
83 the cell wall amidase PcsB [24]. The situation in *S. aureus* is more complex. Complementing
84 WalKR depleted *S. aureus* with constitutively overexpressed autolysins *lytM* or *ssaA* can
85 restore viability but the resultant cells have morphological defects and neither of these genes
86 are themselves essential [7]. The *B. subtilis* extracellular PAS domain of WalK senses
87 peptidoglycan cleavage products generated by autolysins that fall within the WalKR regulon,

88 leading to homeostatic control of cell wall remodelling [25]. The signal sensed by the
89 extracellular PAS domain in *S. aureus* is not known. However, the activity of WalK in
90 staphylococci (and predicted in enterococci) but not in other bacillota is modulated through
91 co-ordination of a divalent metal ion by an intracellular PAS domain [26], raising the possibility
92 of differing roles in regulation beyond peptidoglycan biosynthesis in these genera.

93 The WalKR regulon in *S. aureus* has been determined by comparative transcriptomics
94 by depleting WalKR [8, 13] or by the expression a constitutively active WalR phosphomemetic
95 amino acid substitution (D53E) [27, 28]. These studies, coupled with motif searching using a WalR
96 DNA binding motif defined in *B. subtilis* [12] have built a partial map of the WalKR regulon that
97 includes genes involved in cell wall homeostasis [8, 13] and virulence [27]. Here, we applied a
98 customised implementation of chromatin immunoprecipitation sequencing (ChIP-seq), to
99 define a 17bp *S. aureus* WalR consensus-binding motif. Using this motif to scan
100 the *S. aureus* chromosome *in silico*, we found 118 putative intergenic WalR binding regions.
101 We then confirmed that WalR directly controls expression of multiple peptidoglycan
102 hydrolases. However, we also show that WalR directly negatively regulates *ltaS*, encoding an
103 essential protein necessary for the biosynthesis of mature lipoteichoic acid (LTA), and *hup*,
104 encoding the DNA binding protein HU, which is a nucleoid-associated protein involved in DNA
105 supercoiling and is also essential. Furthermore, we found that WalR positively regulates the
106 expression of *rplK*, encoding the essential ribosomal protein L11, *prs*, purine nucleotide
107 salvage/*de novo* synthesis and *dnaA*, which initiates DNA replication. These data connect the
108 regulation of cell division with chromosomal replication in *S. aureus* for the first time and
109 identify pathways outside the regulation of autolysins that explain the essentiality of WalKR.

110

111 ## Results

112 **Defining an *in vivo* WalR regulon using ChIP-seq**

113 The direct regulon of WalR was investigated using chromatin-immunoprecipitation coupled
114 with Illumina sequencing (ChIP-seq). To permit immunoprecipitation, a 1xFLAG-tag was
115 incorporated onto the C-terminus of WalR using a modified anhydrotetracycline (aTc)
116 inducible pRAB11 expression plasmid [29]. To validate functionally, the transcriptome of
117 *S. aureus* NRS384 with chromosomally C-terminally FLAG tagged WalR [26] was compared to Wt
118 NRS384. This strain had a gene expression profile that matched NRS384 Wt during mid-log
119 phase, as determined by RNA-seq (no significant changes in gene expression (0.585 Log_2FC,
120 0.05 false discovery rate (FDR)). Subsequently, FLAG-tagged expression constructs were also
121 made in pRAB11 for three other response regulators with known DNA-binding motifs (HptR,
122 and SaeR, and VraR) [Figure 1A] [30, 31, 32]. The four plasmids and an empty vector control were
123 each transformed into the CA-MRSA USA300 strain NRS384 with the *spa* gene (encoding
124 Protein A) deleted to reduce non-specific IgG-binding. Dose dependant aTc induction was
125 observed (induced at OD600nm = 0.6 for 1h) for *walR* [Figure 1B]. We looked at the impact of
126 increasing aTc concentration on tag-counts (mapped sequence reads for ChIP purified DNA)
127 and selected an aTc concentration of 100 ng/ml for subsequent ChIP-seq experiments [Figure
128 1C]. We then conducted ChIP-seq with each of the four constructs and the empty vector.
129 Initial analysis of the resulting sequence reads revealed a high background of reads mapping
130 across the entire *S. aureus* chromosome. To improve the signal-to-noise ratio for each of the
131 four ChIP-seq experiments, we performed *in silico* subtraction of the read sets for the three
132 non-target response-regulators and the empty vector from the read set for the target
133 response-regulator [Figure S1, Table S1]. This approach led to some of the expected peaks for
134 HptR and SaeR, upstream of *hpt* and *hla*, respectively [Figure 1D, Figure S1] and revealed WalR

135 binding sites upstream of six genes that included autolysins SAUSA300_2249 (*ssaA*),
136 SAUSA300_2506 (*isaA*), SAUSA300_0438 (*sle1*), cell wall cross linked SAUSA300_0136 (*sasD*),
137 hypothetical secreted SAUSA300_0602, and SAUSA300_0703 (*ltaS*) which encodes
138 lipoteichoic acid (LTA) synthase responsible for polymerising glycerol-6-phosphate into LTA
139 chains [33] [Figure 1D] [Table S1].

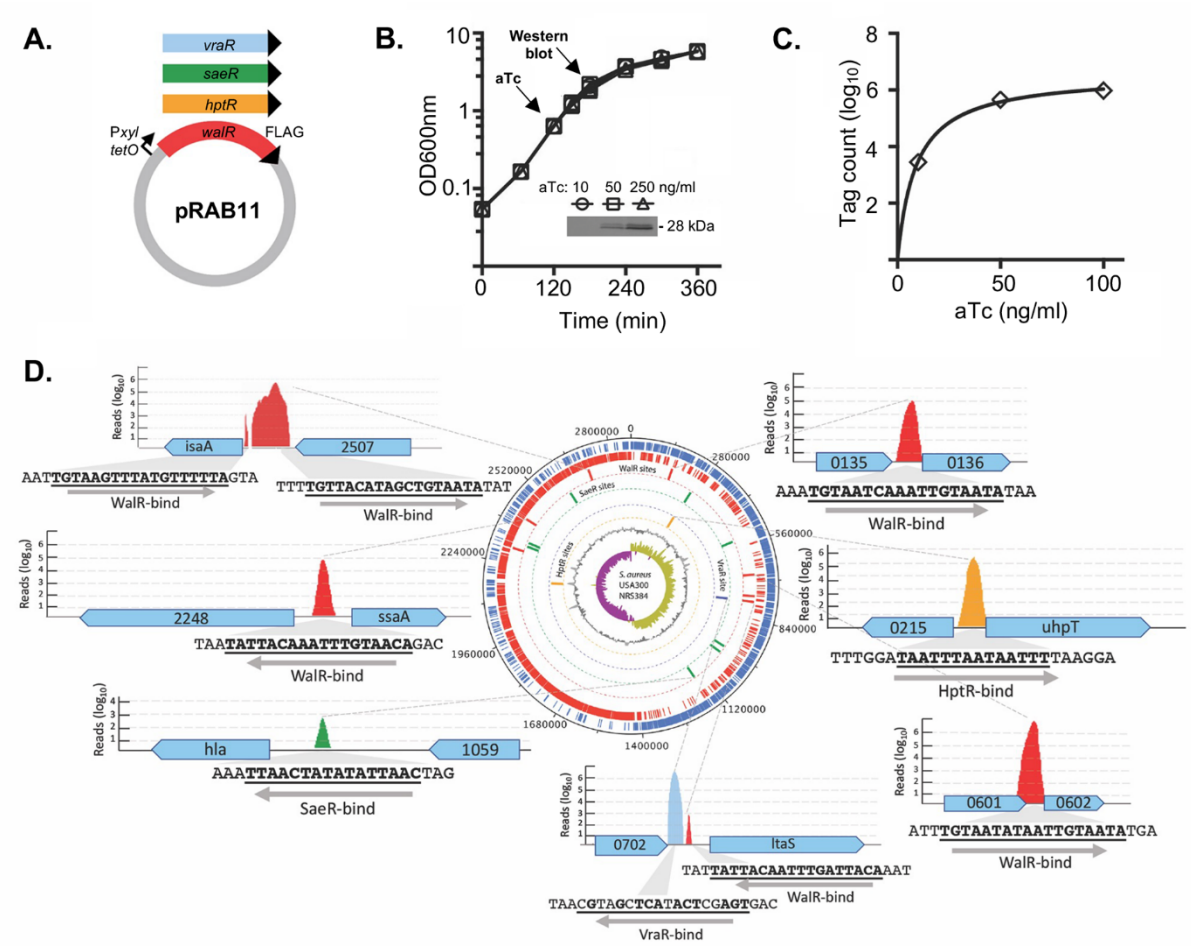

140 ***Figure 1. ChIP-seq analysis of S. aureus WalR chromosome binding sites.*** *A) Four response regulators with C-*
141 *terminal FLAG-tags for immunoprecipitation after induction with anhydrotetracycline (aTc) in S. aureus strain*
142 *NRS384Δspa. B) Dose dependent production of WalR-FLAG (inset Western blot) with increasing concentrations*
143 *of aTc. C) Plot showing increasing numbers of WalR ChIP-seq mapped reads (Tag count) as the aTc concentration*
144 *increases. D) Summary of key ChIP-seq binding sites across the S. aureus chromosome, showing binding motif*
145 *and direction, including four WalR sites, one SaeR, VraR and HptR site.*

146

147 All of these genes were previously identified members of the WalKR regulon [8, 27]. For
148 VraR, we observed a ChIP-seq binding site upstream of *ltaS*, that was adjacent to the putative
149 WalR-binding site [Figure 1]. A total of 22 WalR ChIP-seq peaks upstream of 21 genes were
150 identified, with 12 set aside due to small peak size (7-20 nt) and poor peak prediction scores.
151 Two peaks were identified in 16S rRNA genes, but the use of ribosomal RNA depletion
152 precluded interpretation of RNA-seq data (see below) for these loci. The peak upstream of
153 SAUSA300_0681 was not pursued, as no candidate WalR binding sites were identified. The
154 identification of previously known DNA-binding sites for SaeR and HptR indicated that our
155 ChIP-seq approach was identifying authentic DNA-binding regions [Figure 1]. However, we
156 reasoned that the high stringency of our *in silico* subtraction was likely eliminating peaks
157 corresponding to lower affinity DNA binding regions and therefore would not reveal the
158 entirety of the direct WalR regulon. Consequently, we used ChIP-seq defined WalR binding
159 regions in conjunction with previously validated WalR binding sites [13, 27] to generate a 17bp
160 consensus *S. aureus* WalR-binding motif (5'-TGTHH[N]$_6$WGTNDD-3') [Figure S2AB] and
161 conducted an *in-silico* search of the genome for potential WalR binding sites. In total, 118
162 putative intergenic WalR binding sites were identified along the NRS384 chromosome [Figure
163 S2B], 109 of which were within 500 bp of a predicted CDS transcriptional start site [Table S2].
164

165 **Specific mutations in the *walKR* locus increase and decrease WalKR activity.**

166 The essential nature of WalKR means that the locus cannot be deleted for functional analyses.
167 To further explore the WalR regulon, we assembled a panel of mutants with altered WalK or
168 WalR activity. We used two previously described 'down' mutants with decreased WalKR
169 activity; *S. aureus* NRS384 Δ*yycHI*, with the deletion of both WalKR auxiliary proteins (*yycH*
170 and *yycI*) [17], and NRS384 WalR$_{T101A}$, in which second site PknB phosphorylation at residue T101

171 was abolished [34]. Additionally, we selected two 'up' mutants that have increased WalKR
172 activity; NRS384 $WalK_{Y32C}$ with a mutation in the first trans-membrane domain, and NRS384
173 $WalK_{T389A}$ that is predicted to prevent the dephosphorylation of WalR [35]. We then confirmed
174 that each mutant exhibited the expected WalKR 'up' and 'down' phenotypes. 'Up' mutations
175 result in an increased susceptibility to vancomycin and lysostaphin, increased haemolysis,
176 reduced growth rate, and increased autolysis [13, 27, 36]. Both the $WalK_{Y32C}$ and $WalK_{T389A}$
177 exhibited 'up' mutant phenotypes, with $WalK_{T389A}$ showing the most prominent differences,
178 suggesting the highest level of activation [Figure 2A-C].

179 In contrast, 'down' mutants are more vancomycin and lysostaphin resistant, less
180 haemolytic, and less autolytic [13, 27, 36], phenotypes we confirmed for our two 'down' mutants
181 [Figure 2A-C]. Mutants were also tested for heat sensitivity and susceptibility to a panel of
182 antibacterial agents. In *B. subtilis* mutational activation of WalKR leads to a growth defect at
183 elevated temperatures [22]. However, in *S. aureus* we observed the opposite effect; the growth
184 of 'down' mutants was dramatically impacted at 45°C, whereas 'up' mutants were unaffected
185 [Figure S3A]. Mutational activation of WalKR caused a striking increase in susceptibility to
186 oxacillin and tunicamycin, eliciting >16-fold changes in susceptibility to these cell wall
187 targeting agents. Conversely, mutational dampening of WalKR activity caused a small but
188 reproducible (2-fold) decrease in erythromycin susceptibility, but we did not observe
189 erythromycin or lincomycin hypersensitivity upon WalKR modulation as has previously been
190 reported [6, 37]. Susceptibility to compounds targeting other cellular pathways was unchanged
191 [Figure 2D].

192

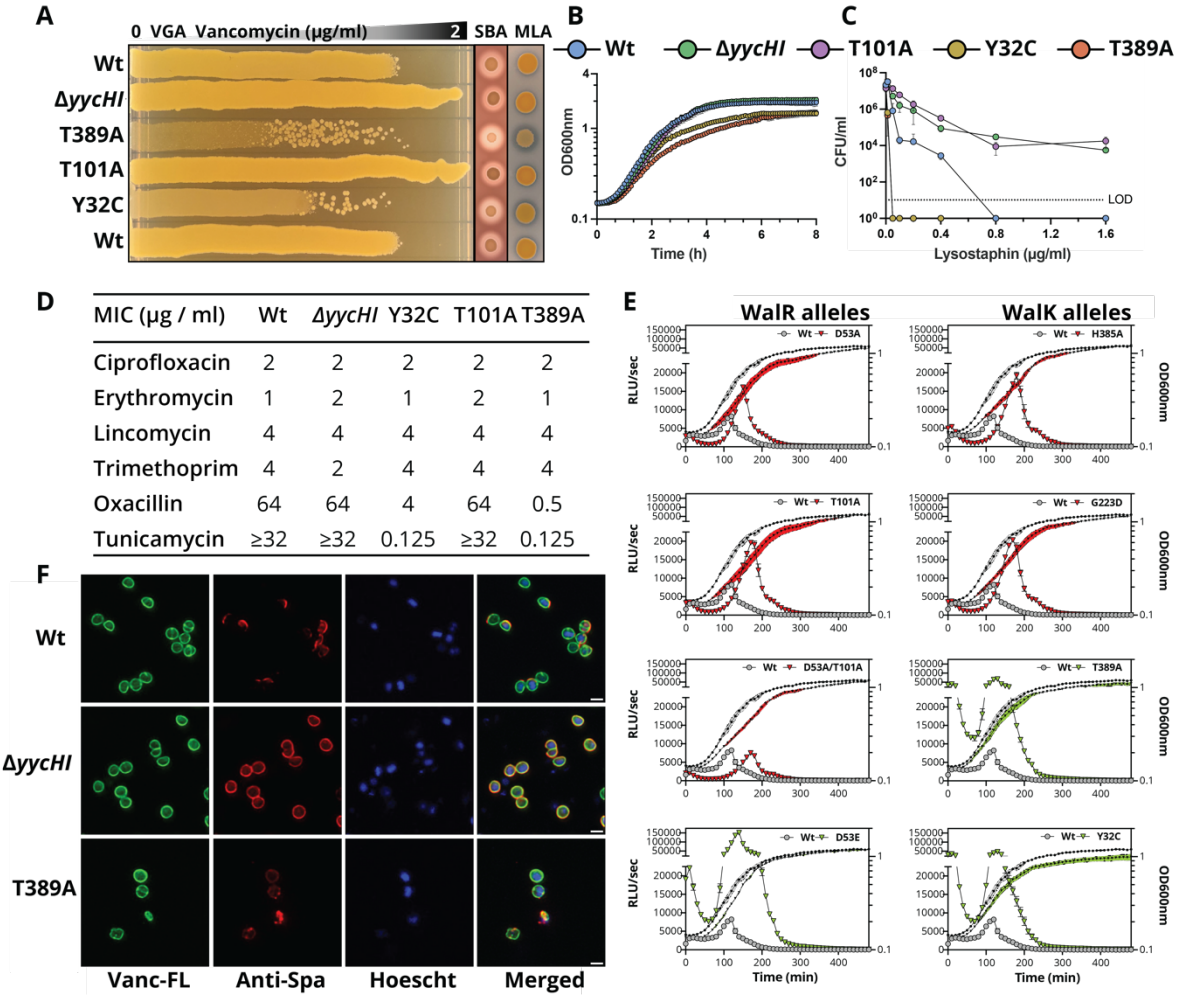

MIC (µg / ml)	Wt	*ΔyycHI*	Y32C	T101A	T389A
Ciprofloxacin	2	2	2	2	2
Erythromycin	1	2	1	2	1
Lincomycin	4	4	4	4	4
Trimethoprim	4	2	4	4	4
Oxacillin	64	64	4	64	0.5
Tunicamycin	≥32	≥32	0.125	≥32	0.125

Figure 2. Phenotypic characterisation of WalKR mutant strains. *A) Vancomycin gradient assay (VGA), sheep blood agar (SBA) Micrococcus luteus agar (MLA) for the comparison of vancomycin susceptibility, haemolysis and Atl mediated autolytic activity, respectively. B) Growth curves, C) Susceptibility to lysostaphin after a 90 min exposure (LOD – Limit of detection) and D) Minimal inhibitory concentration of antibiotics against the different WalKR mutant strains. E) Kinetic split luciferase interaction of native WalR-SmBIT / WalK-LgBIT and WalKR mutant proteins throughout growth in NRS384. OD600nm: black filled circle (WalR/WalK Wt) and filled black triangle (WalR/WalK mutant). RLU: grey filled circle (WalR/WalK Wt) and either red ('down' mutation) or green ('up' mutation) filled triangle. Results are the mean from three independent determinations and the error bars show the standard deviation. F)) Immunofluorescence microscopy showing the impact of WalKR activity on distribution of Protein A and cell morphology in S. aureus. Scale bar is 1 micron.*

204 TCS phosphoryl transfer from the sensor histidine kinase to the cognate DNA-binding
205 response regulator requires direct interaction [38]. To assess this transfer and the impact of the
206 'up' and 'down' mutations on interaction dynamics between WalK and WalR across growth,
207 we implemented the Promega NanoLuc® split luciferase system, as recently described for
208 *S. aureus*, with modifications [39]. Proteins were C-terminally tagged (separated by a glycine
209 serine linker) with either the small bit (SmBIT- 11 amino acids) or large bit (LgBIT – 17.6 kDa)
210 to reconstitute a functional luciferase that emits light in the presence of the furimazine
211 substrate. Our modifications (*S. aureus* codon-optimised luciferase subunits, with expression
212 from two separate plasmids, leaky expression from the Pxyl/tetO* promoter and addition of
213 the substrate to the growth media) allowed the kinetics of protein-protein interaction to be
214 non-invasively measured throughout *S. aureus* growth. Chromosomal C-terminal tagging of
215 WalR-SmBIT and WalK-LgBIT at the native locus showed that the proteins tolerated the
216 presence of either tag, with no growth defect [Figure S3B].

217 We then constructed WalR-SmBIT and WalK-LgBIT fusions in the plasmid system with
218 native and mutant proteins, following cell density (OD600nm) and light emission (RLU)
219 throughout growth. We observed immediate interaction of WalK with WalR upon dilution in
220 fresh media, with the peak interaction in the mid-exponential phase of growth, and
221 subsequent rapid decline of the interaction to undetectable levels (5h) in stationary phase.
222 This pattern was exaggerated in the 'up' mutants with higher light emission throughout
223 growth (including lag phase) for both $WalK_{Y32C}$, $WalK_{T389A}$ or the previously described $WalR_{D53E}$
224 mutant [27, 28] compared to the native WalK/WalR interaction [Figure 2E]. 'Down' mutants
225 including $WalR_{D53A}$ (cannot be phosphorylated by WalK), $WalR_{T101A}$, $WalK_{D53A/T101A}$ and
226 $WalK_{G223D}$ (reduced autophosphorylation and transfer to WalR [40]) exhibited a consistent
227 profile of reduced initial WalK/WalR interaction during lag phase compared to native

228 WalK/WalR. Loss of either D53 or T101 phosphorylation led to a right-shifted peak of
229 interaction, correlating with the reduced growth rate of the 'down' strains [Figure 2E]. D53
230 was dominant over the T101 phosphorylation site, which is consistent with the essentiality of
231 the D53 compared to the T101 residue. Loss of D53 phosphorylation also reduced the total
232 level of WalK/WalR interaction. The kinetic profile of the $WalR_{T101A}$ mutant mimicked the
233 interaction profile of the $WalK_{G223D}$ mutant with a 1.5-fold increase in the maximal level of
234 interaction (compared to native WalK/WalR). This increase correlated with the same mid-log
235 phase time point as seen in the native interaction [Figure 2E]. 'Down' mutants also yielded
236 detectable interactions into stationary phase. These interaction profiles combined with
237 phenotypic profiling validate our panel of 'up' and 'down' mutants.

238 We then used high-resolution immunofluorescence microscopy to assess the impact
239 of *walKR* mutations on *S. aureus* cell morphology and localisation of the well-characterised
240 cell wall cross-linked Protein A [Figure 2F]. Both mutants imaged (Δ*yycHI* 'down' and $WalK_{T389A}$
241 'up') deviated from wild-type morphology and exhibited altered Protein A distribution. In the
242 wild-type, Protein A was found away from the septal planes with defined foci, in agreement
243 with the model of distribution observed for signal sequence containing YSIRK/GS motif
244 surface proteins [41] [Figure 2F]. Whereas cells of the Δ*yycHI* down mutant displayed a more
245 uniform, peri-cellular distribution of Protein A with increased fluorescence per cell [Figure 2F,
246 S3C]. By contrast, the cell wall integrity of $WalK_{T389A}$ was visibly compromised compared to
247 both the wild-type and the Δ*yycHI* 'down' mutant, resulting in low cell circularity [Figure 2F,
248 S3]. WalK activation caused significantly reduced Protein A fluorescence per cell and a change
249 in distribution towards small, discrete foci, suggesting an association with membrane blebs.
250 This contention was reinforced by flow cytometry that showed a large subpopulation of

251 $WalK_{T389A}$ cells reacting with an anti-cell envelope antibody (SA-AF549 [Mu *et al.* 2023 in
252 review]) but lacking DAPI stained DNA [Figure S4].
253
254 **WalKR activation causes a global change in gene expression**
255 To assess the impact of WalKR activation on *S. aureus* gene expression we performed
256 RNA-seq from RNA extracted during exponential phase, comparing $WalK_{T389A}$, the most
257 activate 'up' mutant, to the NRS384 wild type. Activation of WalKR caused a global change in
258 gene expression, with ~55% of genes (1117) undergoing a significant change in expression
259 (FDR $\leq$0.05, $\log_2$FC ≥0.585), of which approximately half (551) were up-regulated and half
260 (564) were down-regulated [Figure 3C]. Activation of WalKR predominantly increased
261 expression (≥1.5 $\log_2$FC, FDR $\leq$0.05) of genes encoding autolysins, virulence factors,
262 membrane transporters, and proteins of the amino acid, purine, and fatty acid biosynthesis
263 pathways [Figure 3A, Table S3]. Genes involved in oxidative stress response, metal ion
264 homeostasis, and protein fate were primarily decreased in expression ($\log_2$FC ≤-1.5, FDR
265 $\leq$0.05) [Figure 3A, Table S3]. Whereas the expression of genes encoding ribosomal proteins,
266 transcription factors, and proteins involved in carbohydrate metabolism, DNA maintenance,
267 and cell wall organisation were both up- and down-regulated (FDR $\leq$0.05, $\log_2$FC ≥1.5 or ≤-
268 1.5)[Figure 3A, Table S3]. Genes predicted to be directly controlled by WalKR, or those
269 identified via ChIP-seq, were not necessarily those that exhibited the largest changes in
270 expression [Figure 3BC].
271 Explanations for two of our observed WalKR phenotypes can be found in the $WalK_{T389A}$
272 RNA-seq data. Firstly, increased haemoylsis [Figure 2A] in $WalK_{T389A}$ mutants is explained by
273 an increase in *hla* expression (+1.7 $\log_2$FC), encoding alpha-toxin, upon WalK activation.
274 Secondly, enhanced zones of clearing surrounding $WalK_{T389A}$ on heat killed *Micrococcus luteus*

275 agar plates [Figure 2A] arise due to increased peptidoglycan degradation by the dual activity

276 autolysin Atl [42] (+2.85 $\log_2$ FC).

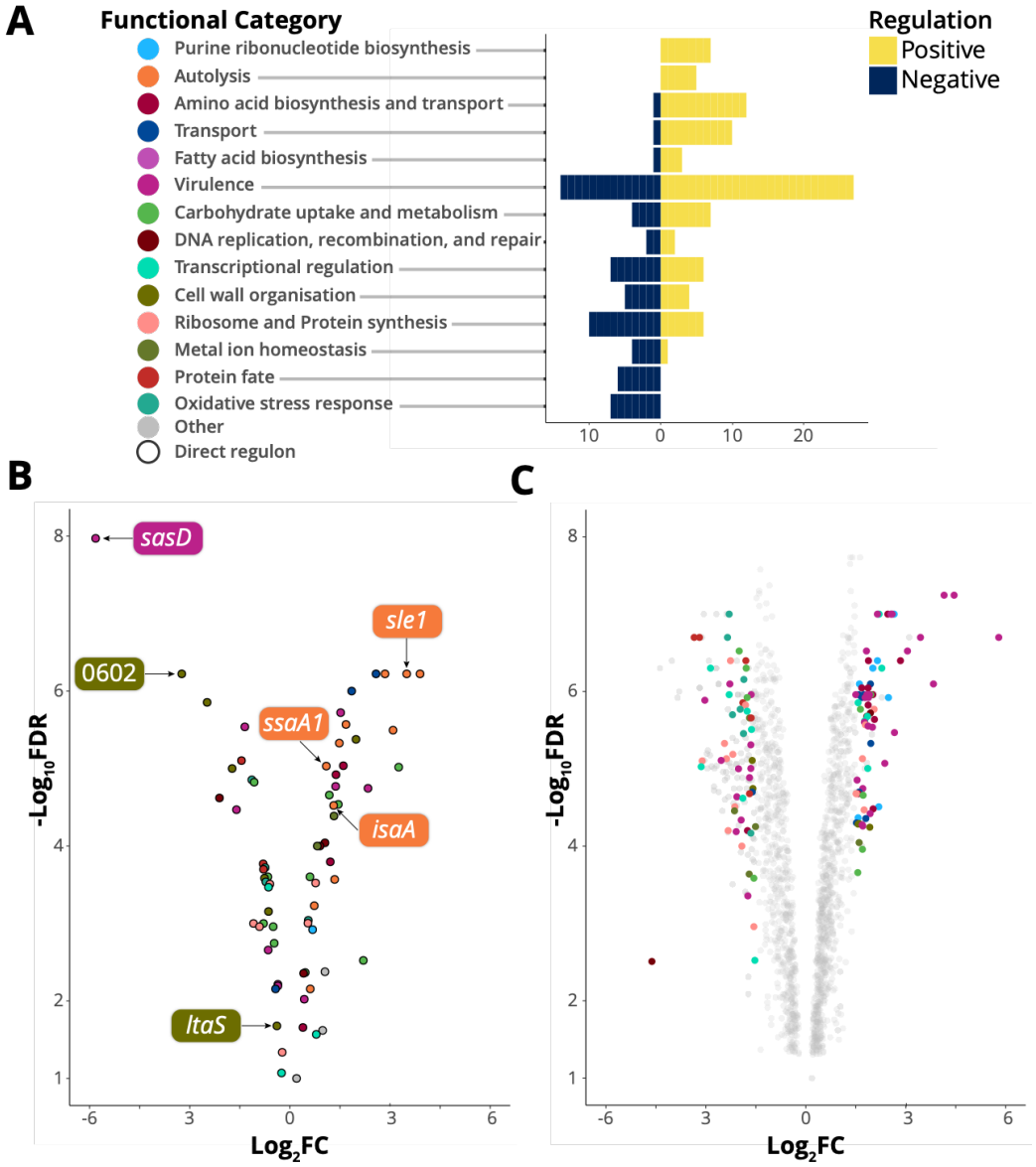

277 ***Figure 3. The direct and indirect WalKR regulon.*** *A) The number of genes in each category that are positively or*

278 *negatively regulated upon WalK activation (FDR ≤0.05, $\log_2$FC ≥1.5 or ≤-1.5). For clarity, categories where n ≤ 2*

279 *are not shown B) Gene expression changes of the predicted direct WalKR regulon upon WalK activation (WT vs*

280 *$WalK_{T389A}$). Genes with WalR binding sites confirmed by ChIP-seq are highlighted. C) Global change in*

281 *transcriptome upon mutational activation of WalK (WT vs $WalK_{T389A}$). Members of gene sets undergoing a $\log_2$FC*

282 *≥1.5 or ≤-1.5 are highlighted. Y-axis labels in panel A serve as the legend for panels B and C.*

283 **Positioning of WalR binding site, not sequence or orientation, dictates of mode of**
284 **regulation.**

285 To investigate whether the sequence of WalR motifs could determine the mode (positive or
286 negative regulation), or degree, of change in gene expression, WalR motif diversity was
287 visualised as a maximum-likelihood phylogenetic tree and the tips labelled with gene
288 expression changes upon WalK activation [Figure S5]. Functional groups of regulated genes
289 were also mapped to examine whether specific motif signatures were linked to gene sets
290 [Figure S5]. We did not observe clustering of positively or negatively regulated genes, nor did
291 branches of the tree correspond to specific gene functions [Figure S2C]. Therefore, the
292 sequence of WalR motifs does not dictate the mode of regulation, nor is it linked to the
293 functional class of the gene it controls.

294 Previous work in *B. subtilis* examined the relationship between the position of WalR
295 binding sites and the promoter regions of a small number of WalR regulated genes, finding
296 that positively regulated genes were predominantly bound upstream of the promoter -35
297 element, whereas negatively regulated genes were bound between -35 and -10 regions [14].
298 Using a similar approach, the positions of WalR binding sites of the direct regulon were
299 mapped in relation to predicted transcriptional start sites and promoters [43] [Table S4]. The
300 orientation of WalR binding site in relation to the downstream gene was not significantly
301 associated with the magnitude (Student's t test, $p = 0.288$) or mode (Chi-squared Test, $p =$
302 0.878) of expression change. However, the position of the WalR binding site did dictate the
303 mode of regulation (Chi-Squared Test, $p = 0.000551$); WalR binding upstream of the -35
304 element was associated with positive regulation, while WalR binding between, or
305 downstream of, -35 and -10 elements was associated with negative regulation [Table S3].

306 Thus, whether WalR activates or represses the expression of a gene is determined primarily
307 by its position relative to the promoter rather than motif sequence.
308

309 **Functional validation of WalR directly regulated genes**

310 WalR binding to promoters of the six loci identified by ChIP-seq was assessed *in vitro* using
311 electrophoretic mobility shift assays (EMSAs) with recombinant WalR [Figure 4A, Figure S6].
312 Fluorescently labelled DNA duplex probes corresponding to promoter regions encompassing
313 WalR binding sites were incubated with increasing concentrations of WalR. All six DNA regions
314 underwent mobility shifts upon addition of increasing concentrations of WalR, demonstrating
315 binding affinity greater than for a non-specific DNA control lacking the WalR binding motif
316 [Figure 4A]. Binding specificity was confirmed by competition experiments; addition of an
317 excess of unlabelled specific duplex abrogated binding, whereas unlabelled non-specific
318 duplex did not [Figure S7]. As the phosphorylation status of recombinant WalR is unknown,
319 the impact of phosphorylation on WalR binding affinity was investigated using
320 phosphomimetic mutations. WalR modified at the WalK phosphorylation site ($WalR_{D53E}$)
321 caused a modest increase in affinity for the two probes tested (p*sle1*, p*sasD*) [Figure S7].
322 However, introduction of a second potential phosphomimetic mutation at a site modified by
323 the serine-threonine kinase PknB [44] ($WalR_{D53E,T101E}$) did not increase binding affinity further,
324 instead reducing affinity to the level of wild type WalR [Figure S7]. This result was
325 corroborated by construction of a chromosomal $WalR_{T101E}$ mutation, which did not yield an
326 'up' mutant but instead decreased WalR activity leading to reduced vancomycin susceptibility
327 (MIC of 4 vs 1 µg/ml in the Wt).
328

329 As a result of ChIP-seq, we also identified VraR binding to the *ltaS* promoter, with the
330 peak overlapping with the consensus VraR binding motif (5'-TGA[N_{1-3}]TCA-3') [30, 45] [Figure
331 S8A]. We then investigated the specificity of WalR and VraR binding within the promoter
332 region of *ltaS*. WalR had no affinity for the duplex encompassing the *ltaS* VraR binding site
333 [Figure S7B]. VraR did exhibit affinity for the WalR binding site, however, this binding was
334 shown to be non-specific by competition assay [Figure S7C]. Therefore, WalR and VraR bound
335 to the *ltaS* promoter at discrete sites dictated by their respective recognition motifs.
336 Following the *in vitro* confirmation of WalR binding to sites identified by ChIP-seq, we
337 sought to assess the impact of WalR binding on *S. aureus* promoter activity [Figure 4B].
338 Promoter regions encompassing the WalR binding motif were transcriptionally fused with
339 yellow fluorescent protein (YFP) in the promoter-less pIMC8-YFP vector. To assess the impact
340 of WalR activity on gene expression, each construct and a paired WalR binding motif mutant
341 (first TGT in WalR motif mutated to CCC) were transformed into NRS384. Additionally, the
342 native promoter construct was transformed into NRS384 Δ*yycHI* ('down' mutant) and
343 $WalK_{Y32C}$ ('up' mutant). The $WalK_{Y32C}$ strain was chosen rather than $WalK_{T389A}$, as suppressor
344 mutants arose in this background through genetic instability, which was not observed in
345 $WalK_{Y32C}$. As a positive control, we included the promoter for the *hpt gene* encoding the
346 glucose-6-phosphate transporter which is responsive to the presence of glucose-6-phosphate
347 [32] [Figure 4B]. Strains were grown to stationary phase with fluorescence and CFU determined.
348 From the RNA-seq data, half the genes were upregulated by WalKR activation (*sle1*, *ssaA* and
349 *isaA*), and half downregulated (*sasD*, *ltaS,* and SAUSA300_0602) [Figure 4B]. Of the down
350 regulated genes, all exhibited increased fluorescence upon abrogation of the WalR binding
351 motif, showed increased fluorescence in the Δ*yycHI* mutant, and decreased fluorescence in
352 the $WalK_{Y32C}$ background, indicative of their negative regulation by WalR [Figure 4B]. For

353 upregulated genes, abrogation of the WalR motif reduced fluorescence, with increased
354 fluorescence in $WalK_{Y32C}$ and decreased fluorescence in the Δ*yycHI*, indicative of positive WalR
355 regulation [Figure 4B]. As the *isaA* and *ssaA* promoter regions contain two WalR binding
356 motifs, both were individually mutated. For *isaA*, the WalR binding site closest to the TSS
357 (CCCI, 37 bp to TSS) caused the greatest decrease in promoter activity [36], whereas for *ssaA*,
358 only the more distal binding site (CCCII, 167 bp from the TSS) reduced expression, which
359 corresponded to the ChIP-seq peak for *ssaA* [Figure 1D].

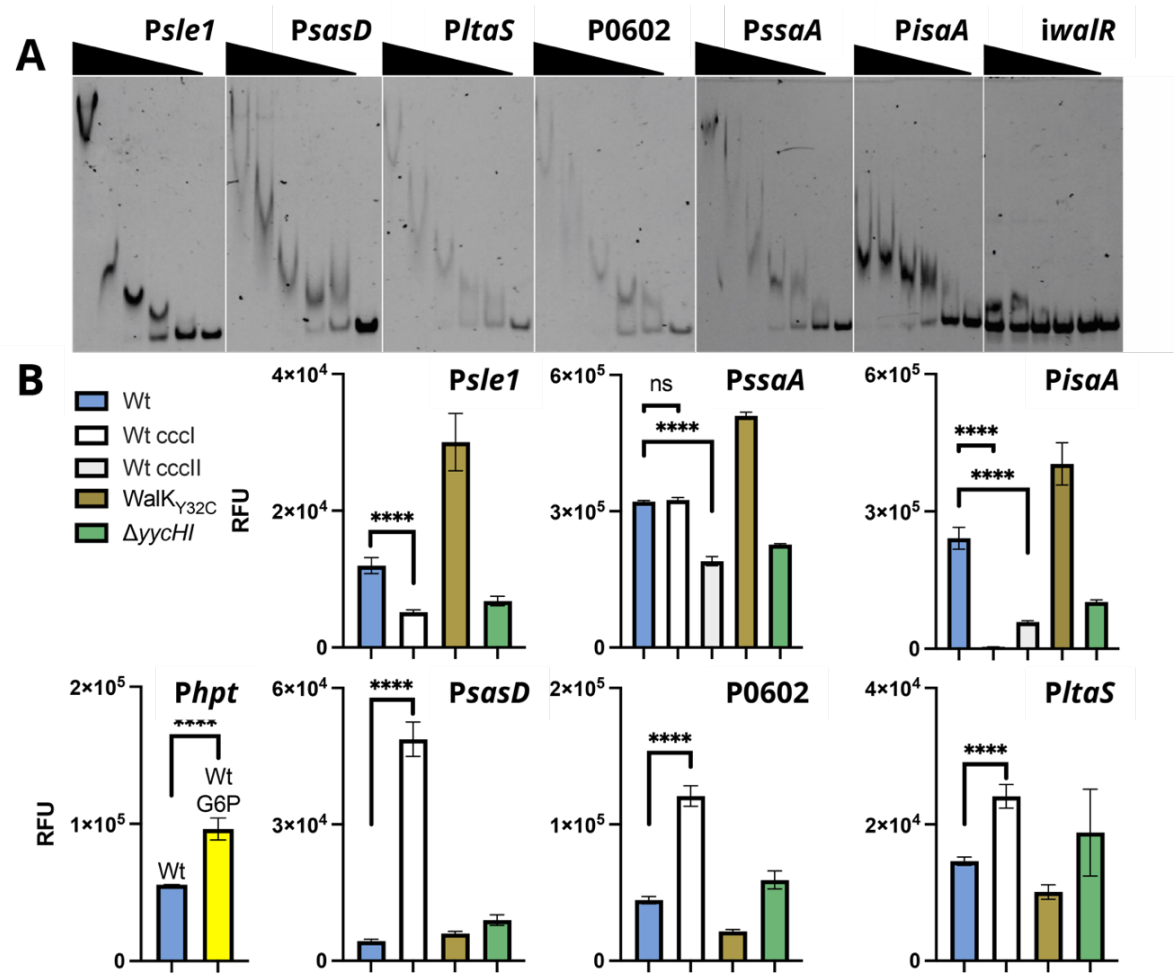

360 ***Figure 4. In vitro and in cellulo confirmation of WalR regulation.*** *A) Dose dependent band shifts caused through*
361 *specific WalR binding to the ChIP-seq identified promoter regions. An intragenic region of the walR gene was*
362 *used as a non-specific control (iwalR). A total of 5 doubling dilutions (plus a no protein control) of WalR (starting*
363 *at 20µM for all except PssaA where 40 µM) was used. B) Cumulative YFP fluorescence of S. aureus reporter strains*

364 *from stationary phase cultures. The glucose-6-phosphate (G6P) inducible hpt gene was used as a positive assay*
365 *control through addition of 25µM of G6P. Promoter activity was assessed in wild type NRS384, with or without*
366 *an abrogating (ccc) mutation in the WalR binding site. The native promoter construct was also analysed in*
367 *$WalK_{Y32C}$ (up mutant) or ΔyycHI (down mutant). Results are means from three independent experiments with the*
368 *error bars showing the standard deviation of the mean. The significance of the CCC mutation was determined*
369 *using an unpaired Student's t test; ns: not significant, <0.0001: **** versus the Wt promoter in NRS384.*
370

371 **Control of essential genes by WalKR**

372 To investigate WalKR essentiality in *S. aureus* and triage genes for further analysis based on
373 their likely contribution to the essentiality phenotype, we analysed intersecting data sets
374 where genes fulfilled the following criteria: (i) contain a predicted upstream WalR-binding site
375 (ii) belong to the core *S. aureus* genome, (iii) are essential for growth in rich media, and (iv)
376 their expression is significantly changed upon WalK activation as defined by RNA-seq [Figure
377 5A]. We found that within the predicted direct WalR regulon, seven essential genes undergo
378 a significant change in gene expression upon activation by WalKR (FDR $\leq$0.05, $\log_2$FC ≥0.585)
379 [Figure 5AB]. These genes were *dnaA*, *hup, ltaS, prs, and rplK, tagG,* and *tarF*; encoding
380 chromosomal replication initiator protein DnaA, the sole DNA-binding protein HU,
381 lipoteichoic acid synthase, ribose-phosphate pyrophosphokinase (purine salvage/de novo
382 synthesis), ribosomal protein L11 (50S subunit component), teichoic acid biosynthetic
383 proteins TagG and TarF, respectively [Figure 5B]. Additionally, three essential genes had a
384 predicted upstream WalR binding site but did not undergo a significant change in expression:
385 *dnaD*, *rnz*, and *sufB*, encoding putative replication restart protein DnaD, ribonuclease Z, and
386 FeS assembly protein SufB. Of these essential genes, a ChIP-seq peak was identified upstream
387 of *ltaS* and *dnaD* [Figure 5A].

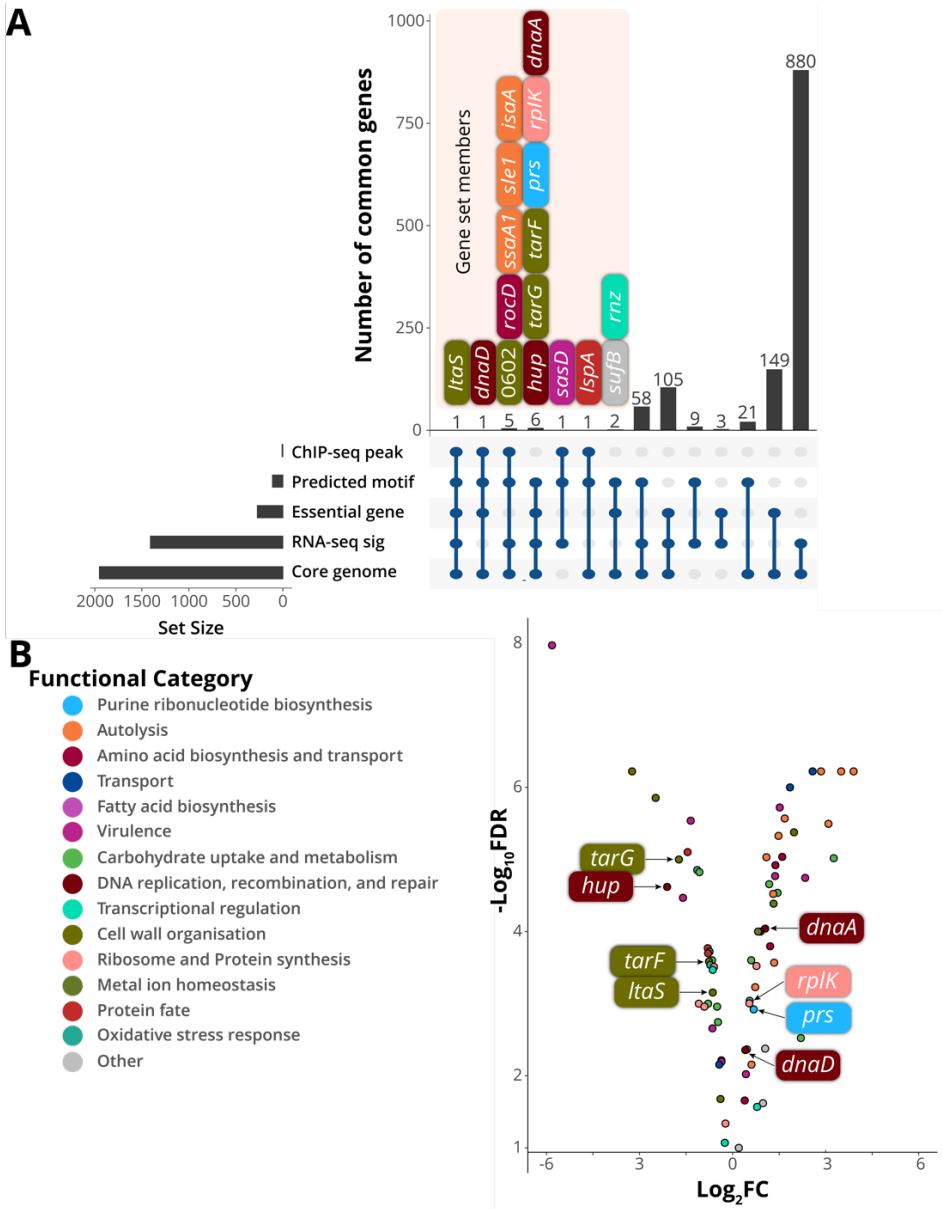

Figure 5. Analysis of putative WalR controlled essential genes. *A) Intersections between essentiality analysis and -omics data displayed as an UpSet plot. Members of gene sets where n<10 are shown. RNA-seq sig is RNA-seq significance (FDR <0.05, log2FC ≥0.585). B) Gene expression changes of the predicted direct WalKR regulon upon WalK activation (WT vs WalK$_{T389A}$). Essential genes with predicted WalR binding sites are highlighted.*

S. aureus WalKR directly controls *five* essential genes

To further characterise the seven essential genes within the predicted direct WalR regulon (*dnaA, hup*, *ltaS*, *prs, rplK, tarF, and tarG*) [Figure 6AB, Table S2], we next built a time-resolved

396 picture of their expression. The *dnaD* locus was also included in the analysis due to functional
397 links between DnaD and DnaA previously described in *B. subtilis* [46, 47]. The promoter regions
398 for these genes, with or without an abrogating mutation (TGT to CCC) in the WalR-binding
399 site, were introduced into a luciferase reporter plasmid and transformed into *S. aureus*
400 NRS384. The resulting *S. aureus* strains were monitored for growth and light emission every
401 10 min over an 8 h period. For comparison, promoters from the previously characterised WalR
402 regulated genes and the *walR* gene itself were included [Figure 6A]. Expression from the *walR*
403 promoter rapidly peaked in mid-exponential phase and then tapered off, as has been
404 observed previously [48] [Figure 6A]. The previously ascribed WalR regulation of the six ChIP-
405 seq hits were corroborated by the luciferase reporter assays; mutation of the WalR binding
406 site yielded a significant reduction in the level of expression throughout growth for the
407 positively regulated genes (*sle1, ssaA* and *isaA*). While an increased level of expression was
408 observed in the negatively regulated genes upon mutation of the WalR binding site mutation
409 (*sasD*, SAUSA300_0602 and *ltaS*). Loss of the WalR negative regulation was shown to relieve
410 repression of *sasD,* while the impact on SAUSA300_0602 was most pronounced into
411 stationary phase of growth. Only a subtle difference in expression was observed for *ltaS*;
412 mutational abrogation of WalR binding prevented "turning off" of gene expression, resulting
413 in prolonged expression into stationary phase [Figure 6A]. We then examined the impact on
414 the additional essential genes identified from the analysis of the direct regulon. No regulation
415 was detected for *tagG, tarF* or *dnaD.* However, the very low level of *dnaD* and *tarF* promoter
416 activity under the conditions tested precluded a definitive determination. Whereas a strong
417 positive regulation was observed for *rplK. prs* was also shown to be positively regulated*. hup*
418 was shown to be weakly negatively regulated by WalR, which caused a reduction in the
419 expression upon the transition into stationary phase, similar to *ltaS*. For hup there was a bi-

420 phasic change at 190 min present in the Wt which was lost when the binding site was

421 mutated.

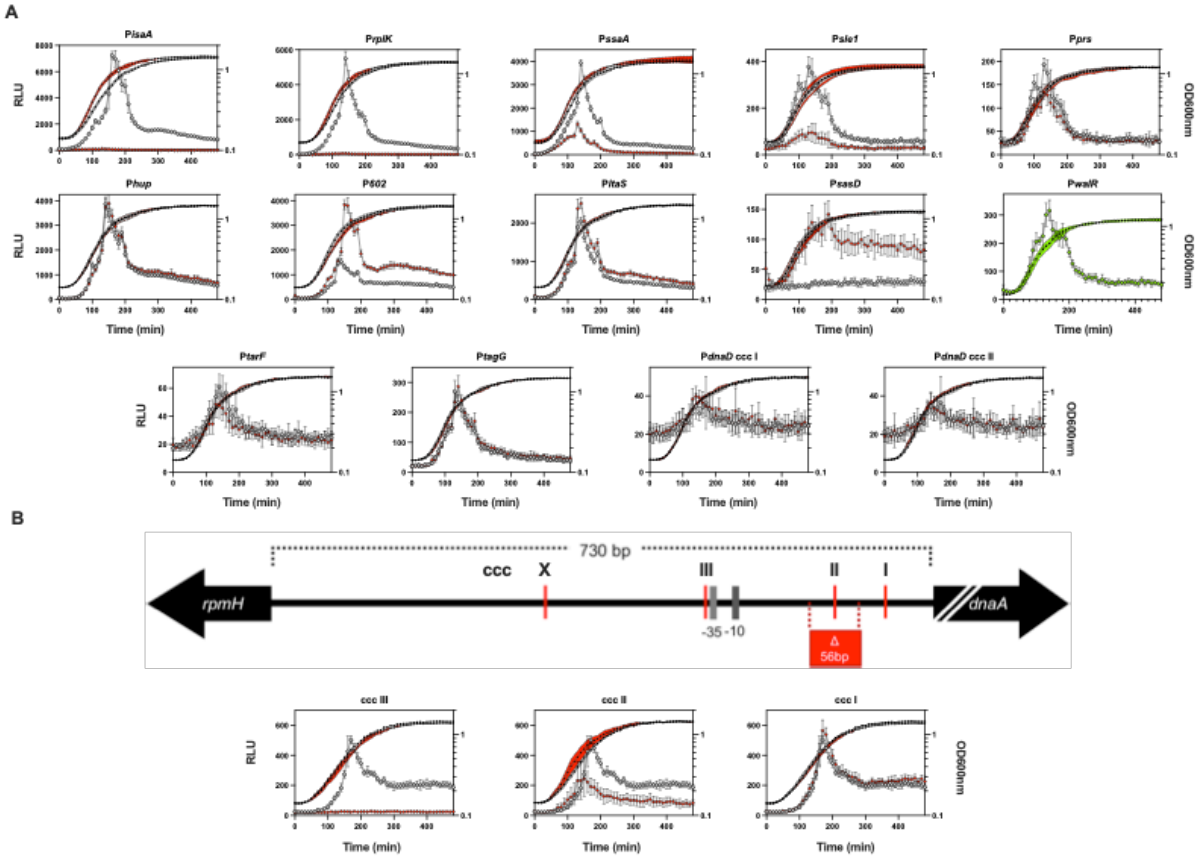

422 ***Figure 6: Temporal control of essential genes by WalR.*** *A) Luciferase reporters (pIMK1-LUX) showing the*

423 *changes in promoter activity of the Wt (open grey circle: relative light units (RLU); filled black circles: OD600nm)*

424 *or the ccc (open red diamond: relative light units (RLU); filled black diamond: OD600nm) mutated WalR binding*

425 *site in LB media over time. Results are the combined means from three independent experiments and the error*

426 *bars showing the standard deviation. The expression profile for walR is shown in green open circles and growth*

427 *in filled black circles. B) Schematic of the dnaA promoter region with four identified WalR motifs denoted (to*

428 *scale except dnaA is truncated). The Wt and the three dnaA motif mutants (ccc I to ccc III, with site X not*

429 *examined) were analysed as described above. The 56bp deletion previously identified to reduce DnaA mediated*

430 *DNA replication [49] is highlighted, as are the -35/-10 boxes for the dnaA promoter [43].*

431

432 Closer inspection of the large (730 bp) upstream intergenic region between the
433 divergent *dnaA* and *rpmH* genes revealed an enrichment of potential WalR binding motifs
434 upstream of *dnaA* [Figure 6B]. The three sites proximal to the dnaA gene were chosen for
435 further analysis (site X excluded, Figure 6B). From reporter analysis, sites ccc II and ccc III
436 impacted the expression of *dnaA* while no change in expression was observed for the
437 mutation of ccc I [Figure 6B]. We observed both a negative regulation for ccc II and a complete
438 abrogation of expression for ccc III, suggesting a complex fine tuning of *dnaA* expression
439 afforded by WalR. Recently, a suppressor mutant with a deletion in the *dnaA* promoter that
440 reduced the level of DnaA activity (initiation of DNA replication) was identified in a *S. aureus*
441 *Δnoc* strain [49]. This deletion removed a 56 bp region surrounding the WalR binding site
442 denoted by ccc II [Figure 6B]. Here, in agreement with this previous observation, we identified
443 the reduced expression from the *dnaA* promoter upon abrogation of the ccc II WalR binding
444 site.
445
446 **Modulation of WalKR activity alters LTA structure and susceptibility to Congo red**
447 The physiological impact of negative *ltaS* regulation by WalR was assessed by extraction of
448 the LtaS product, lipoteichoic acid (LTA), from strains of differing WalKR activity grown to
449 stationary phase. LTA is an anionic polymer composed of a repeating chain of glycerol
450 phosphate units anchored to the cell membrane via a diacylglycerol group and decorated with
451 side chain modifications of D-alanine and/or glycosyl moieties [50]. Analysis of LTA extracted
452 from cells by polyacrylamide gel electrophoresis (PAGE) yields a distinctive laddered banding
453 pattern, with each subsequent band representing a polymer chain length of n + 1 [51]. The
454 degree of side chain modification can also be observed, where high levels of heterogenous
455 modification cause a smearing pattern and loss of single band resolution [51]. LTA derived from

456 cells with differing levels of WalKR activity (NRS384, NRS384 Δ*yycHI*, NRS384 $WalK_{T389A}$)
457 revealed alterations to LTA structure upon activation of WalKR. Activation of WalKR resulted
458 in changes to LTA chain length, with a reduction in mid-length LTA [Figure 7A, orange line]
459 and increase in high molecular weight LTA [Figure 7A, black line]. Additionally, LTA from
460 NRS384 with wild-type or decreased WalKR activity gave a characteristic smeared banding
461 pattern, indicating a high-degree of side-chain modification, whereas activation of WalKR
462 resulted in LTA with clear, single band resolution, showing a reduction in side-chain
463 modification. Analysis of the LTA content in the supernatant showed that activation of WalK
464 (NRS384 $WalK_{T389A}$) caused a large increase in LTA shedding, consistent with prior
465 observations of the strains compromised cell wall and membrane blebbing [Figures 2E, S4].
466
467 Subsequently, we investigated the impact of modulating WalKR activity on the
468 susceptibility to Congo red, an azo dye reported to inhibit LtaS [52]. Typically, titration of a drug
469 target will alter susceptibility to that drug, with an inverse relationship between target
470 expression level (amount of target) and the resultant level of susceptibility [53]. Based on this
471 principle, we predicted that WalKR up mutants, in which *ltaS* expression is reduced would be
472 more susceptible to Congo red. However, we observed the opposite effect, with activation of
473 WalKR decreasing susceptibility to the dye, while a reduction in WalKR activity increased dye
474 susceptibility [Figure 7B].

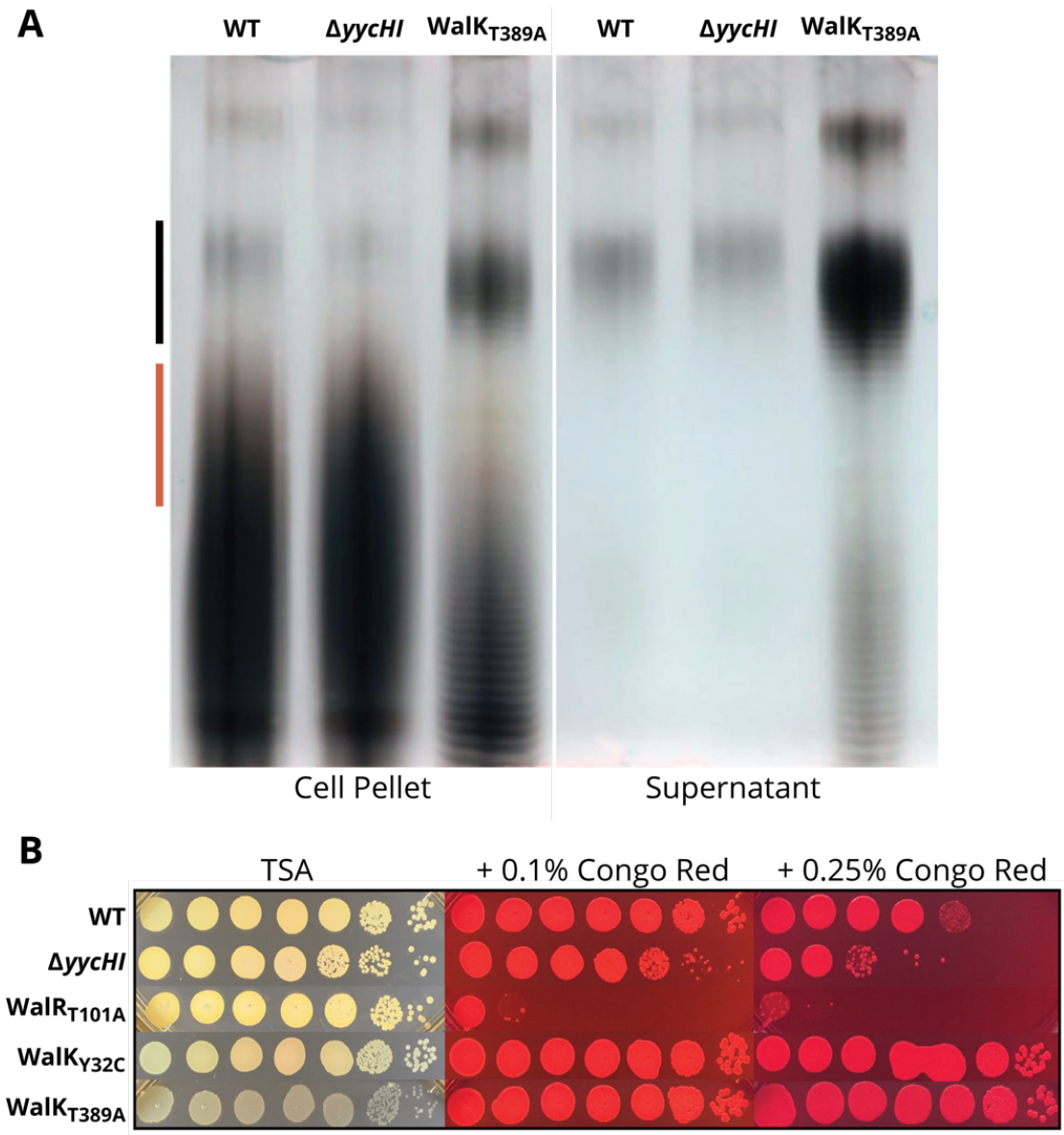

475 ***Figure 7.*** *PAGE analysis of purified LTA from NRS384 isogenic mutants. Each band indicates a glycerol phosphate*
476 *polymer length of n+1. Black and orange lines indicate regions of difference between mutants. B) Activity of*
477 *Congo red against isogenic NRS384 mutants. Spots result from serial dilution of cultures grown overnight to*
478 *saturation and plated onto TSA with varying amounts of Congo red.*

479

480 **WalR controls DNA compaction through regulation of DNA binding protein HU**

481 The second essential gene that was *lux* reporter validated as negatively regulated by
482 WalR was *hup,* encoding the sole DNA-binding protein HU in *S. aureus*. Belonging to a family
483 of low molecular weight nucleoid-associated proteins (NAPs), the function of *S. aureus* HU is

484 largely uncharacterised, although its structure has been determined [54]. However, HU NAP
485 orthologs from other bacteria have previously been shown to control DNA compaction,
486 introducing negative supercoils into relaxed DNA [55, 56] and, recently, the *B. subtilis* HU
487 ortholog (HBsu) was shown to play an essential role in the initiation of DNA replication [57]. To
488 investigate potential changes in DNA topology mediated by *S. aureus* HU and WalR regulation
489 of HU, we performed CRISPRi knockdown of *walR, hup,* and, as a negative control, *hla*. The
490 CRISPRi knockdown titrated the expression of each targeted gene [Figure 8A], resulting in 57x,
491 20x, and 78x fold downregulation of *hup*, *walR*, and *hla* respectively with the highest
492 concentration of inducer tested. A degree of knockdown in the absence of inducer indicated
493 "leaky" expression of the CRISPRi guide or due to the location of the guide for *hup*.

494 Due to the small size of the *hup* gene, only two guide RNAs could be designed, with
495 one targeting the middle of the 270 bp gene (non-functional) and the second functional guide
496 overlapping the start codon/promoter region. Knockdown of HU resulted in a relaxation of
497 plasmid supercoiling, evidenced as an increase in DNA band intensity during chloroquine gel
498 electrophoresis, resulting from more slowly migrating topoisomers in comparison to the
499 empty vector control [Figure 8A pSD1 vs pSD1*hup*, white up arrow]. In contrast, knockdown
500 of *walR* had the opposite effect, increasing the intensity of DNA bands resulting from
501 topoisomers with higher supercoiling density that migrate faster through the gel [Figure 8A
502 pSD1 vs pSD1*walR*, white down arrow], consistent with the negative regulation exerted over
503 HU by WalR. As expected, knockdown of *hla* or the empty vector had no impact on DNA
504 topology [Figure 8A pSD1 vs pSD1*hla*]. These results show that *S. aureus* HU, as observed in
505 other bacteria, increases the supercoiling density of DNA. We propose that the negative
506 regulation of *hup* by WalR has the opposite effect, causing the relaxation of supercoiling and
507 leading to decreased compaction of cellular DNA.

508 **Changes in initiation of DNA replication mediated by WalR and HU**

509 HBsu is essential for the initiation of DNA replication in *B. subtilis*, with depletion of
510 the protein resulting in the reduction of the *ori*-to-*ter* ratio equating to reduced DNA
511 replication. This is measured by whole genome sequencing using genomic DNA extracted
512 from cells during exponential growth [57]. This technique provides an indication of the number
513 of chromosome replication origins per cell [49, 57]. To assess whether modulation of *hup* could
514 also impact the initiation of DNA replication in *S. aureus*, we applied the same genome
515 sequencing approach to our CRISPRi knockdown constructs of *walR, hup, hla* and empty
516 vector with either, 0 or 100 ng/mL aTc induction. Calculation of mean *ori*-to-*ter* ratios based
517 on quadruplicate biological replicates for each of the four constructs revealed the expected
518 phenotypes, with a significant reduction in the *ori*-to-*ter* ratio from around 2.60 for the empty
519 vector or non-target *hla* control compared to a mean ori-ter of 2.15 when the expression of
520 *hup* was repressed [Figure 8BC]. This compared with a significant increase above the controls
521 of the *ori*-to-*ter* ration to 2.88 when *walR* was repressed [Figure 8BC], consistent with our
522 earlier finding that WalR negatively regulates *hup* expression [Figure 6A]. Additionally,
523 knocking down WalR expression could directly impact *dnaA* expression through alleviating
524 the negative regulation exerted through WalR binding sites ccc I/ccc IV in the *dnaA* promoter.
525 These experiments suggest that *S. aureus* HU plays an important role in the direct regulation
526 of DnaA to promote initiation of DNA replication, as recently reported for *B. subtilis* [58].
527

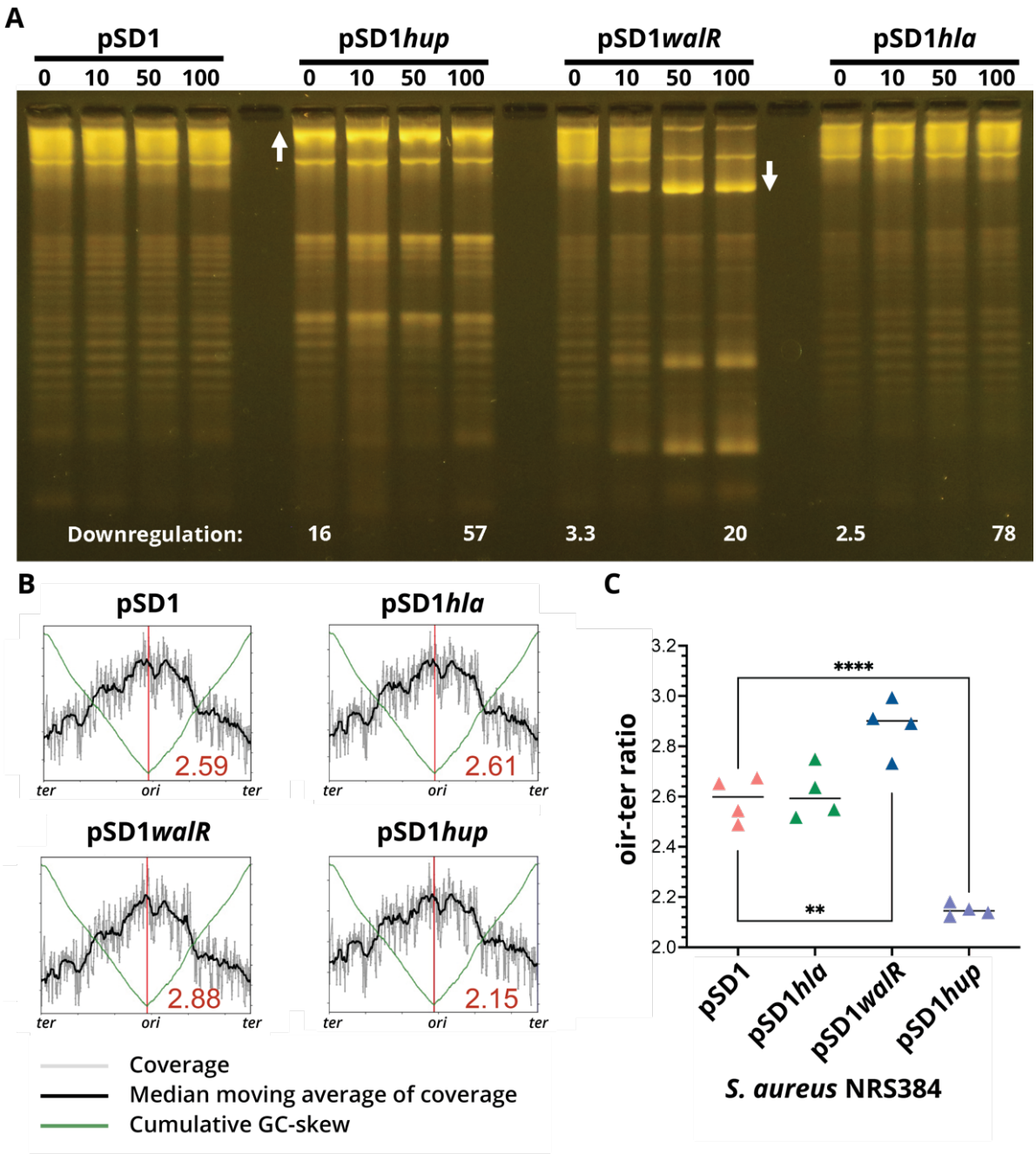

528 ***Figure 8. Impact of CRISPRi mediated downregulation of hup or walR on DNA topology.*** *A) NRS384 containing*
529 *either pSD1 (empty vector), pSD1hup, pSD1walR or the negative control pSD1hla were induced with increasing*
530 *concentrations of aTc (0, 10, 50 and 100 ng/ml) to knockdown expression. At 5h post induction total RNA and*
531 *plasmids were isolated. Plasmids were run on a 1% TBE gel containing 2.5 µg/ml chloroquine to allow for the*
532 *resolution and visualisation of discrete topoisomers of supercoiled plasmid DNA. Relative fold downregulation of*
533 *each targeted gene compared to uninduced vector control (pSD1, 0) as determined by RT-qPCR is denoted at the*
534 *bottom of the image. The image is representative of three repeat experiments. B) A representative whole genome*

535 *sequencing read-coverage graph showing the ori-ter ratios for the four CRISPRi constructs under 100 ng/mL aTc*
536 *induction. Each plot represents one of four biological sequencing replicates for each CRISPRi construct. Shown in*
537 *the bottom right quadrant of each graph is the mean ori-ter ratio across the four replicates. The ori-ter ratio*
538 *between the sequence read coverage at the origin and terminus of replication is also called peak-to-trough ratio,*
539 *PTR. C) Summary graph of ori-ter ratios for each of the four CRISPRi constructs induced with 100 ng/ml of aTc to*
540 *downregulate expression of the three targeted genes (hla, walR and hup). Shown are the mean of quadruplicate,*
541 *independent biological replicate sequencing experiments. Differences between means assessed using an*
542 *unpaired student's t test, **p=0.0059, ***p=<0.0001.*

543

544

545 ## Discussion

546 It has been over two decades since the characterisation of temperature sensitive
547 mutants led to discovery of the *walKR* (then *yycFG*) locus in *B. subtilis* [10] and shortly afterwards
548 in *S. aureus* [6]. In the intervening years, a substantial body of work has characterised this TCS
549 in several Bacillota genera, finding the locus to be both highly conserved and ubiquitously
550 essential [6, 10, 59, 60, 61, 62]. Although there are differences in the WalKR regulon between species,
551 its core is made up of genes controlling cell wall metabolism, primarily those that encode
552 autolysins or hydrolase inhibitors [11, 13, 61]. In *S. aureus*, a series of seminal papers mapped the
553 staphylococcal WalKR regulon and found that activation of the system positively controls
554 expression of a suite of virulence genes in addition to the repertoire of autolysins required for
555 maintaining peptidoglycan homeostasis [8, 13, 27]. More recently, an elegant study using a strain
556 deleted in all TCSs other than WalKR described the regulon in isolation, without crosstalk from
557 other TCSs, and found control of a smaller set of genes, including autolysins but not the
558 virulence genes controlled by SaeR [28].

559 Here, for the first time in *S. aureus*, we use ChIP-seq to define the WalKR regulon from
560 a starting point for direct mapping of WalR binding to chromosomal DNA within the
561 bacterium. Subsequently, we used these data to generate a *S. aureus* specific WalR consensus
562 binding motif and to inform physiologically relevant cut-offs for interrogating transcriptomic
563 data obtained when mutationally activating WalK. These experiments allowed us to define a
564 direct and indirect WalKR regulon. Our results confirm and expand the pioneering discoveries
565 of Dubrac and Msadek *et al*., with WalKR directly regulating several genes encoding autolysins
566 and activation of the system leading to increased expression of many virulence genes [8, 13, 27].
567 Additionally, consistent with our earlier work [63], we observed upregulation of a variety of
568 genes involved in central metabolism upon WalK activation, particularly those involved in
569 amino acid, purine, and fatty acid biosynthesis. Filtering our results to identify essential genes
570 directly controlled by WalKR in *S. aureus*, we identify and characterise new members of the
571 WalKR direct regulon; *rplK*, *hup, ltaS, prs* and *dnaA*. Of which, *prs* and *rplK*, belong to the
572 central metabolic pathways of purine and protein biosynthesis respectively.

573 We find that WalKR negatively regulates the expression of *ltaS,* dampening expression
574 of the gene from late exponential into stationary phase. To our knowledge, this is the first
575 report of direct transcriptional regulation of *ltaS*, although post-translational regulation
576 through cleavage of the extracellular enzymatic domain has been described [64]. We also
577 detected VraR binding to a second site further upstream in the *ltaS* promoter. We note that
578 *ltaS* has been previously mapped to the VraR regulon though comparative transcriptomics
579 that found upregulation of the gene on VraR activation [65]. However, direct control was not
580 demonstrated, as this was prior to the identification of polyglycerol phosphate synthase
581 activity in *S. aureus* [33]. The fact that WalKR and VraSR regulate *ltaS* transcription is perhaps
582 not surprising. Both TCSs are intimately connected to cell wall homeostasis, with WalKR

583 maintaining a balance of peptidoglycan autolysis that allows the cell to grow but not lyse [11,
584 16], and VraSR governing the cell wall stress stimulon in response to extracellular insult [66, 67].
585 Together, LTA and wall teichoic acid are present in the Gram-positive cell wall in roughly equal
586 proportion to peptidoglycan [68]. Modulation of *ltaS* expression by two TCSs that integrate
587 different signals, alongside post-translational regulation of the enzyme, presumably ensures
588 tight and finely tuned control of *ltaS* activity, enabling co-ordination of LTA synthesis with
589 peptidoglycan remodelling.

590 We observed a change to LTA structure upon activation of WalK, consisting of
591 alterations to LTA chain length and a reduction in LTA modification. As LTA chain length is an
592 intrinsic property of the LtaS enzyme that is dictated by the availability of lipid starter units
593 [69], it is unlikely that the chain length differences observed upon activation of WalK are solely
594 attributable to direct negative regulation of *ltaS*. We speculate that the global transcriptional
595 rewiring of the cell upon WalK activation may affect the availability of lipid starter units,
596 although this remains to be investigated. After LTA structure analysis, we aimed to use the
597 posited *ltaS* inhibitor Congo red as a tool to probe *ltaS* activity in WalKR mutants [52]. However,
598 contrary to our expectation that activation of WalKR, and therefore down regulation of *ltaS*,
599 would increase Congo red susceptibility, we observed an increase in susceptibility to Congo
600 red of WalKR down mutants. Although this did not match our prediction, similar results have
601 been recently reported, with laboratory evolution of VISA strains showing increased Congo
602 red susceptibility in strains with and without WalKR mutations [70, 71]. We propose that Congo
603 red susceptibility arises due to genotype-naïve pleotropic effects of the VISA phenotype on
604 cell wall structure, limiting its utility as a direct *ltaS* probe in this instance.

605 In addition to its role in teichoic acid biosynthesis, we found that WalKR controls
606 essential genes involved in initiation of DNA replication. In *S. aureus*, DNA replication is
607 initiated by binding of DnaA to AT-rich regions at the origin of replication, *oriC* [72]. This process
608 is tightly controlled, as mistiming of initiation results in aberrant cell division [73]. Here we find
609 that WalKR can both positively and negatively regulate the expression of *dnaA* and negatively
610 regulates *hup.* The role of *hup* in staphylococcal DNA replication initiation has not previously
611 been investigated but in *B. subtilis hup* homologue *hbs* has been shown to promote initiation
612 [74]. Here, we find that this function is conserved in *S. aureus*; knocking down expression of *hup*
613 resulted in reduced initiation of DNA replication. In addition to *hup,* two other regulators of
614 DNA replication initiation have been characterised in *S. aureus*; Noc and CcrZ [73]. Noc is a
615 negative regulator of DnaA driven initiation [49], whereas CcrZ is a positive regulator [73]. The
616 mechanisms underlying DnaA control by these proteins are yet to be fully defined, however
617 it is unlikely that Noc directly regulates *dnaA* expression [49] and CcrZ may act post-
618 translationally, by phosphorylating an unknown intermediate factor [73]. In a recent dissection
619 of the role of Noc in *S. aureus*, a suppressor mutant down regulating the activity of DnaA was
620 identified with a deletion of a 56bp region [Figure 6B] within the 5'UTR of *dnaA* [49]. As this
621 region encompasses one of two characterised WalR binding motifs upstream of the gene, we
622 propose that the loss of positive WalR control through deletion of the binding site explains
623 the observed decease in DnaA activity. Additionally, RNA-seq showed an overall increase in
624 *dnaA* expression (1.05 Log_2FC - $WalK_{T389A}$ vs Wt) in exponential phase upon WalK activation,
625 further highlighting the positive role WalR has on *dnaA* expression.

626 That WalR was found to positively regulate *dnaA* and negatively regulate *hup*, both of
627 which are promoters of initiation, is somewhat counterintuitive. Knockdown of *walR*
628 expression caused under-initiation, consistent with its negative control of *hup* but

629 contradictory to its positive regulation of *dnaA*. It may be that loss of HU is a dominant
630 phenotype, reducing initiation even in the presence of higher levels of DnaA, or alternatively,
631 that regulation of each gene is temporally distinct. The latter hypothesis is supported by our
632 observation that *dnaA* regulation occurred during exponential phase whereas regulation of
633 *hup* was in stationary phase. However, exactly how WalKR transcriptional regulation of both
634 *dnaA* and *hup* works in concert with post-translational control mediated by HU, Noc and CcrZ
635 to ensure tight, spatiotemporally accurate, control of initiation of DNA replication remains to
636 be elucidated. It is of note that during the discovery of WalR in *B. subtilis* using a temperature-
637 sensitive mutant, anucleate cells were observed at the non-permissive temperature. This
638 observation hints at the possibility of a wider association between WalR and DNA replication
639 in other Bacillota [10].

640 HU is a multifunctional protein, in addition to its role in DNA replication initiation, it
641 also contributes to DNA compaction, introduces negative supercoils into DNA [55] and can
642 impact localised gene regulation [75]. As we observed opposite changes to DNA supercoiling
643 caused by depletion of *walR* and *hup*, we propose that the negative regulation of HU by WalR
644 causes relaxation of supercoiling and may lead to decreased compaction of cellular DNA.
645 Transcriptional regulation of *hup* expression has not previously been described in *S. aureus*.
646 However, qualitative western blots have shown HU to be continuously present in the
647 staphylococcal nucleoid throughout all growth phases [76]. Taking this into account, we propose
648 that WalKR regulation of *hup* is not a binary switch, but rather provides tuneable control of
649 this essential system. Intriguingly, in *Mycobacterium tuberculosis* the serine/threonine kinase
650 PknB negatively regulates HU DNA binding through phosphorylation [77] and in *S. aureus*, PknB
651 mediated phosphorylation activates WalR [44]. Furthermore, a PknB phosphorylation site on
652 HU has been experimentally identified in *S. aureus* [78]. Therefore, PknB may directly repress

653 HU DNA binding through post-translational modification and indirectly represses *hup*
654 expression through activation of WalR.

655 The reason for essentiality of WalKR differs across Bacillota species [79]. In *S. aureus,*
656 essentiality is proposed to result from polygenic control of non-essential autolysins involved
657 in the cleavage and relaxation of peptidoglycan crosslinks, allowing expansion of the cell wall
658 [7]. Here, we extend this hypothesis, showing WalKR direct control of at least five essential
659 genes (*rplK*, *hup, ltaS, prs* and *dnaA*) not directly involved in peptidoglycan biosynthesis but
660 intimately linked with cell growth and cell division. Thus, we propose that WalKR essentiality
661 arises though polygenic co-ordination of multiple cellular processes; ribosome assembly,
662 peptidoglycan homeostasis, LTA polymerisation, DNA topology, and the initiation of DNA
663 replication, ultimately making WalKR an indispensable link between cell wall homeostasis and
664 DNA replication. We propose a model in which WalK senses an unknown ligand during
665 logarithmic growth through its extracytoplasmic PAS domain, resulting in
666 autophosphorylation, dimerisation, and maximal interaction between WalK and WalR [Figure
667 9AB]. The level of WalK activation can also be dynamically tuned in response to the metalation
668 state of the intracellular PAS domain [36]. WalR:WalK interaction allows phosphotransfer to
669 WalR residue D53, whilst a second WalR site T101 can be phosphorylated through the PknB
670 kinase (recognises muropeptide fragments[80]). Phosphorylated WalR binds the cognate
671 recognition motifs of its direct regulon as a dimer, causing either negative or positive changes
672 to gene expression, primarily dependent on the position of the binding motif in relation to
673 the transcriptional start site [Figure 9B]. The direct WalR regulon has three broad functions;
674 i) control of cell wall metabolism through regulation of a suite of autolysins governing
675 peptidoglycan homeostasis and fine tuning of LTA biosynthesis through negative regulation
676 of lipoteichoic acid synthase; ii) linking initiation of DNA replication to cell wall homeostasis

677 through regulation of *dnaA* and *hup*; iii) signal amplification through modulation of
678 transcription factors, selected other TCSs, and via negative regulation of DNA binding protein
679 HU [Figure 9C]. Together with the downstream effects of changes in cell wall metabolism,
680 signal amplification drives changes in expression of the indirect WalKR regulon, producing a
681 large shift in cellular transcription that includes the increased expression of virulence factors
682 and metabolic genes [Figure 9C].

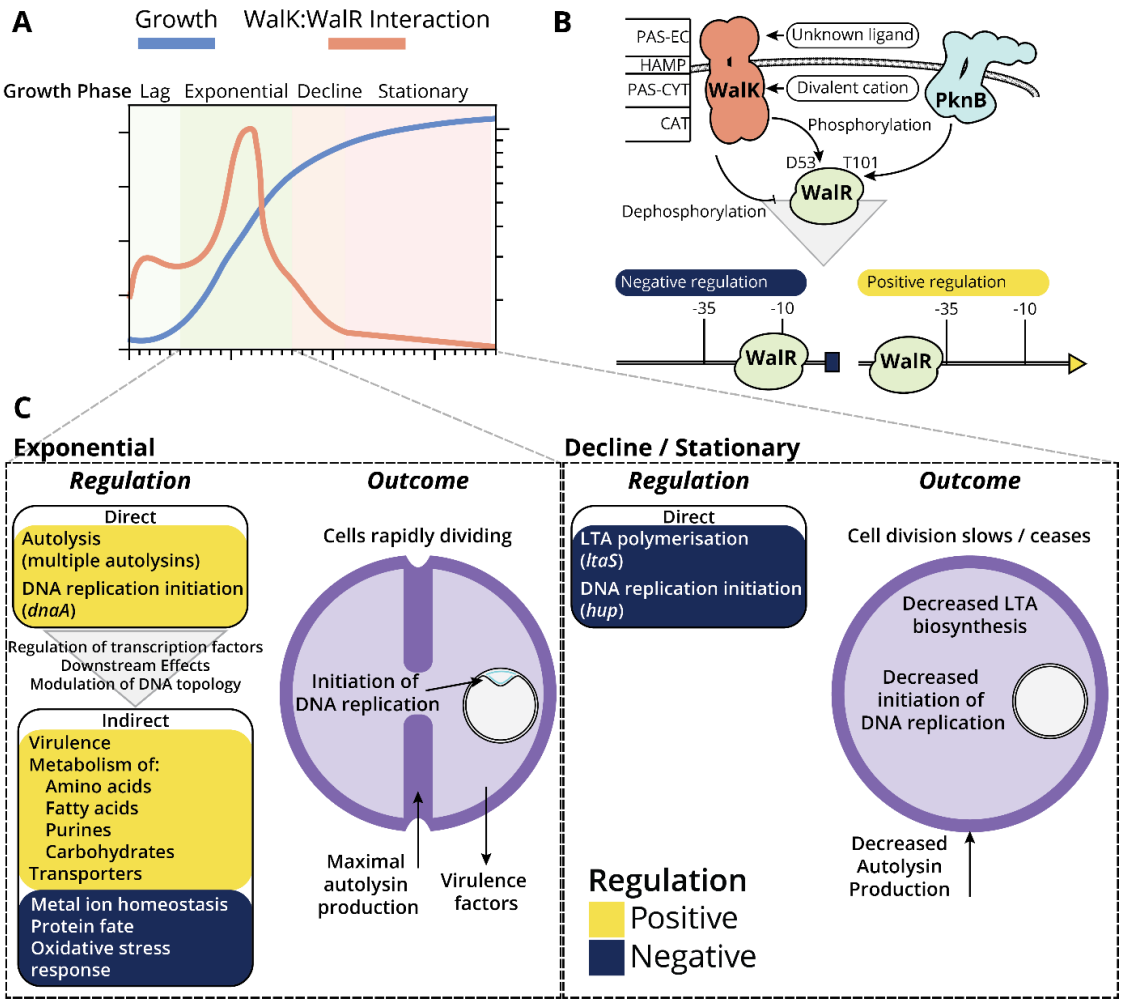

683 **Figure 9. A model of the role of WalKR in cell division.** *A) Changes in the interaction of WalK with WalR*
684 *throughout growth. B) Mechanism of signal transduction and transcriptional control of WalKR. -35 and -10*
685 *denote promoter regions. PAS: Per-Arnt-Sim, HAMP: present in Histidine kinases, CAT: catalytic domain. C)*
686 *Transcriptional changes and their outcomes for the direct and indirect WalKR regulon during different growth*
687 *phases. Yellow and dark blue denote positively, and negatively, regulated gene sets respectively.*

688 WalKR has long been considered a promising target for the development of novel anti-
689 Gram-positive agents [81], although to date no WalKR targeted compounds have been
690 successfully developed. Despite this, the system remains a viable target for conventional
691 antibacterial chemotherapy due to its role as a signal integrating nexus of essential cellular
692 functions and the presence of two PAS domains capable of binding small molecules inside and
693 outside of the cell [16, 36]. Increasingly, alternative strategies to traditional antibacterial
694 chemotherapy are being explored, including the development of so called "antibiotic
695 resistance breaking (ARB) compounds" that re-sensitise resistant strains to existing antibiotics
696 [82, 83].

697 Here, we found that mutationally activated WalKR 'up' mutants were more sensitive
698 to three different antibiotic classes targeting the cell wall: oxacillin, tunicamycin, and
699 vancomycin. In contrast, recent work conducted using the methicillin sensitive *S. aureus*
700 (MSSA) strain ATCC29213 found the opposite; a WalKR 'down' mutation ($WalR_{T101M}$)
701 increased tunicamycin sensitivity [84]. Tunicamycin is a dual targeted antibiotic, binding to MraY
702 and TarO, which belong to the peptidoglycan recycling and wall teichoic acid synthesis
703 pathways respectively [85]. In *S. aureus* ATCC29213, decreased WalKR activity results in indirect
704 downregulation of enzymes within the peptidoglycan recycling *mupG* operon, as well as direct
705 downregulation of autolysins. Together these gene expression changes starve MraY of
706 precursor molecules, making the enzyme exquisitely sensitive to tunicamycin [84]. In *S. aureus*
707 NRS384 the genes of the *mupG* operon were not differentially regulated upon WalKR
708 activation. Consequently, we conclude that tunicamycin sensitivity in NRS384 'up' mutants
709 likely arises through a different mechanism. More broadly, differences in the indirect WalR
710 regulon between MRSA and MSSA may reflect regulatory adaptions necessary to
711 accommodate the exogenous, *mecA* encoded, PBP2a transpeptidase into the complex

712 process of cell wall homeostasis [86]. Here, we found that mutational stimulation of normal
713 WalKR activity rendered NRS384 MRSA susceptible to oxacillin despite the presence of *mecA*,
714 opening an alternative avenue for future WalKR focused drug development; the discovery of
715 ARB compounds that phenocopy WalKR activating mutations.

716

717 ## Materials and Methods

718 **Strains, oligonucleotides, media, and reagents**

719 Bacterial strains and plasmids are listed in Table S5. Oligonucleotides (IDT) used in this study
720 are listed in Table S6. *Escherichia coli* were routinely cultured in LB (Merck) or on L-agar (1.5%
721 [w/v] agar added) unless stated otherwise. *S. aureus* were routinely grown on BHI agar (Bacto,
722 BD Biosciences) or Sheep blood agar. When cultured in broth, they were grown in Brain heart
723 infusion broth Trypticase soy broth (TSB, Oxoid), or LB with shaking at 200 rpm. For selection,
724 antibiotics (Sigma) were added at the following concentrations for *E. coli* (*E.c*) and *S. aureus*
725 (*S.a.*): Ampicillin 100 µg/ml – *E.c.*, Kanamycin 50 µg/ml – *E.c./S.a.*, Chloramphenicol 10 µg/ml
726 – *E.c./S.a*. Restriction enzymes, Phusion DNA polymerase, and T4 ligase were purchased from
727 New England Biolabs. Phire Hotstart II DNA polymerase for colony PCR was purchased from
728 Thermo Fisher.

729

730 ***S. aureus* site-directed mutagenesis by allelic exchange**

731 Upstream and downstream regions of the point mutation for *walK*^{T389A}
732 (IM7/IM120/IM121/IM10), *walR*^{T101A} (IM31/IM232/IM233/IM10) or *spa* deletion
733 (IMT275/IMT353/IMT354/IMT278) were PCR amplified and then a SOE-PCR was performed
734 on the gel extracted template to generate an amplicon for SLiCE cloning into pIMAY-Z [87]. This

735 yielded plasmids pIMAY-Z *walK*^{T389A}, pIMAY-Z *walR*^{T101A} and pIMAY-Z Δ*spa*. To construct
736 pIMAY-Z *walK*^{Y32C}, genomic DNA from a sectored mutant of NRS384 Δ*yycHI* (containing an
737 additional *walK*^{Y32C} mutation) was amplified with primers IM107/IM10 and the amplicon
738 cloned as described above. Construction of isogenic mutants of NRS384 by allelic exchange
739 was performed as described previously [87]. The WalK enhancing mutations could visually be
740 discriminated from the wild type due to reduced colony size and opacity. For the WalR^{T101A},
741 the mutation was screened by colony PCR (70°C annealing temperature) with primers
742 IM233/IM181. From putative mutants, genomic DNA was extracted from 1 ml of overnight
743 culture (DNeasy Blood and Tissue Kit—Qiagen) pre-treated with 100 µg of lysostaphin (Sigma
744 cat. no. L7386) and sequenced on an Illumina NextSeq by the Doherty Applied Microbial
745 Genomics facility (University of Melbourne). Resultant reads were mapped to a NRS384
746 reference genome [88] and mutations identified using Snippy
747 (https://github.com/tseemann/snippy).

748

749 **Construction of pRAB11-FLAG**

750 To construct a vector for the C-terminal FLAG tagging of *S. aureus* proteins, the
751 anhydrotetracycline inducible vector pRAB11 [29] was digested with KpnI to linearise and gel
752 extracted. The 6.4kb vector was then amplified with primers IM512/IM513 to add in a
753 consensus ribosome binding site (IM512), a 1xFLAG tag and downstream *tonB* transcriptional
754 terminator (IM513). The amplimer was digested with KpnI, gel extracted, re-ligated to yield
755 pRAB11-FT. The sequence of the plasmid was verified by sequencing on the Illumina platform.
756 To clone into pRAB11-FT, the vector was digested with KpnI, gel extracted and used as
757 template with primers IM514/IM515 to amplify the vector backbone. Response regulators

758 (WalR - IM516/IM517), (SaeR - IM518/IM519), (VraR - IM520/IM521), (HptR - IM522/IM523)
759 were amplified from the start codon and omitting the stop codon with NRS384 genomic DNA.
760 The products were gel extracted, SLiCE cloned into amplified pRAB11-FT and transformed into
761 IM08B, yielding pRAB11:*walR*^{FLAG}, pRAB11:*saeR*^{FLAG}, pRAB11:*vraR*^{FLAG} and pRAB11:*hptR*^{FLAG}.
762 The plasmids were electroporated into NRS384Δ*spa*.

763

764 **Construction of pIMC8-YFP reporter strains and assay for YFP activity.**

765 Promoter regions for *sasD* (IM1127/IM1107), *sle1* (IM1108/IM1109), *P602* (IM1129/IM1110),
766 *ltaS* (IM1111/IM1112), *ssaA* (IM1130/IM366) *isaA* (IM1128/IM364 were PCR amplified from
767 NRS384 genomic DNA and gel extracted. The vector pIMC8-YFP [36] was digested with KpnI, gel
768 extracted and PCR amplified with IM1/IM385. The amplified promoters and vector were SLiCE
769 cloned, transformed into IM08B and subsequently electroporated into NRS384, NRS384
770 Δ*yycHI* or NRS384 *walK*^{Y32C}. Mutations disrupting the WalR motif (1st TGT to CCC) were
771 introduced by SOE-PCR with the bracketed primers sets for *hpt* (IMT300/IMT301); *sle1*
772 (IM1108/IM1115; IM1114/1109), *P0602* (IM1129/1119; IM1118/IM1110), *ltaS*
773 (IM1111/IM1117; IM1116/IM1112), *ssaA*^{CCCI} (LS371/LS376; LS375/LS372), *ssaA*^{CCCII}
774 (LS371/IM1121; IM1120/LS372), *isaA*^{CCCI} (IM1128/IM1123; IM1122/IM364), *isaA*^{CCCII}
775 (IM1128/IM1125; IM1124/IM364). The resultant mutated promoters were gel extracted,
776 SLiCE cloned, transformed into IM08B and subsequently electroporated into NRS384. For the
777 *sasD* promoter the mutation was incorporated into the reverse primer (IM1113) in
778 combination with IM1127. To assess YFP production, each strain was grown in 5 ml of LB
779 containing 10 µg/ml chloramphenicol in a 50 ml tube for overnight at 37°C with shaking at
780 200 rpm. The culture was diluted 1:100 in 5 ml of fresh LB containing chloramphenicol and

781 incubated overnight. The fluorescence (excitation 512 nm, emission 527 nm) of each strain
782 (200 µl – Nunc black well plates) was read in triplicate using an Ensight multimode plate
783 reader (PerkinElmer) set to 100 flashes per well. Resultant data was plotted using the
784 GraphPad Prism (v9.3.1) software package.

785

786 **Production and purification of proteins.**

787 For production of WalR, Rosetta 2 (DE3) pET28(a):*walR* was grown in 2 L of autoinduction
788 media [89] at 25°C for four days with vigorous shaking, and cells were harvested by
789 centrifugation. For production of VraR Rosetta 2 (DE3) pET21(d): *vraR* was grown in 2 L of LB
790 at 37 °C with vigorous shaking to an OD600 nm of 0.6, chilled on ice for 10 min then induced
791 with 1 mM IPTG. Subsequently, cells were grown for a further 16-20 h at 18 °C with vigorous
792 shaking and harvested by centrifugation. For purification of both proteins, cell pellets were
793 resuspended at 3 ml/ g in buffer A (50 mM NaH_2PO_4 [pH 8.0]) with 300 mM NaCl and 10 mM
794 imidazole. To enhance lysis and prevent proteolysis, 7000 U chicken egg-white lysozyme
795 (Sigma), two complete EDTA-free protease inhibitor tablets (Roche) and 20 U DNase I (NEB)
796 were added. Cells were lysed by sonication and lysates were clarified by centrifugation at
797 30,000 x *g* for 30 minutes at 4°C. The cleared lysate was loaded onto a 25 mL free-flow gravity
798 column (GeneFlow) packed with 3 ml TALON® Metal Affinity Resin (Takara Bio), washed with
799 10 column volumes (CV) of buffer A containing 20 mM imidazole and 2 M NaCl. The protein
800 was eluted in 2 CV of buffer A containing 150 mM imidazole and 300 mM NaCl and dialysed
801 overnight 6 kDa MWCO, CelluSep) into storage buffer (25 mM Tris [pH 8.0], 300 mM NaCl,
802 20 mM KCl, 10 mM $MgCl_2$, 1 mM DTT, 5% glycerol). The proteins were spin concentrated to 5

803 mg / ml (3 kDa MWCO, vivaspin 20, Sartorius), aliquoted, snap frozen in liquid nitrogen, and
804 stored at -80°C until required.

805

806 **Electrophoretic mobility shift assays (EMSAs)**

807 DNA duplex probes for electrophoretic mobility shift assay binding assays were generated by
808 annealing two 70 bp single-stranded oligonucleotides, one of which was labelled with Cy5
809 fluorophore on the 5' end (Table S6). Annealing was performed in duplex buffer (30 mM
810 HEPES [pH 7.5], 100 mM potassium acetate) by heating equimolar concentrations of
811 complimentary single-stranded oligonucleotide at 94°C for two min and then cooling to room
812 temperature over 30 min. Duplexes were subsequently gel-extracted from a 2% (w/v) agarose
813 1xTBE gel. Binding reactions were performed in a final volume of 25 µl of binding buffer
814 (25 mM Tris [pH 8.0], 300 mM NaCl, 20 mM KCl, 10 mM $MgCl_2$, 1 mM DTT, 4 µg BSA, 0.5 µg
815 salmon sperm DNA). Initially, varying concentrations of WalR/VraR were incubated for 5 min
816 at 25°C in binding buffer, then DNA probe was added to a final concentration of 16 nM and
817 the reaction was incubated for a further 15 min. After incubation, reactions were mixed (5:1)
818 with 6x Orange G loading buffer [90] and 5 µl was electrophoresed on an 8% polyacrylamide
819 native gel (29:1 acrylamide:bisacrylamide ratio) in 1xTBE at 4 °C. Bands were visualised using
820 a GE Amersham 600 imager in the Cy5 channel with a 10 min exposure time.

821

822 **Total RNA extraction and rRNA depletion**

823 A 10 ml LB (50 ml tube) culture was grown overnight at 37°C with shaking at 200rpm. The
824 saturated culture was diluted 1:100 into fresh 10 ml TSB and grown to an OD600nm of 0.8-

825 1.0. A 5 ml aliquot of culture was removed and added to 10 ml of RNAprotect Bacteria Reagent
826 (Qiagen) and mixed by vortexing. The sample was incubated at room temperature for 5 min.
827 Cells were then harvested by centrifugation (7,000*xg*/5min/22°C), the supernatant discarded
828 and the cell pellet resuspended in 1 ml of TRIzol (Invitrogen). Cells were lysed by bead beating
829 (Precellys 24 instrument - 6000 rpm, 1 min, 100 µm zirconium beads) and cell lysates were
830 clarified by centrifugation (20,000*xg*/10 min/4°C). Subsequently, 700 µl of supernatant was
831 removed and mixed with 700 µl of ethanol. RNA was extracted using a Direct-Zol RNA
832 miniprep plus kit (ZymoResearch) according to manufactures instructions, including the on-
833 column DNase I treatment step. Following RNA extraction, an additional DNA removal step
834 was performed using a TURBO DNA-free kit (Invitrogen) according to manufacturer's
835 instructions. The absence of DNA was accessed *by gyrB* PCR (IM1020/IM1021) on 1µl of RNA
836 template, yielding no amplification. RNA quality was determined on the Bioanalyser (Agilent)
837 with all yielding a RIN score of above 8. For each strain three independent RNA extractions
838 were made. A 5 µg aliquot of total RNA was depleted for rRNA with the mRNA then converted
839 into cDNA with the Scriptseq complete bacteria kit (Epicentre). The libraries were sequenced
840 on the Illumina HiSeq platform for 50 bp single end reads.

841

842 **RNA-seq data analysis**

843 RNA-seq data was analysed using the *S. aureus* USA300 FPR3757 reference genome
844 (accession number: NC_007793) and Kallisto [91], a kmer based pseudoalignment tool, with
845 analysis and visualization using Degust [https://github.com/drpowell/degust]. Degust uses
846 Voom/Limma [92] and generates an interactive website to analyse and explore the data.

847

848 **Preparation of samples for ChIP-seq**

849 An overnight culture (10 ml LB in 50 ml tube) of each strain NRS384Δ*spa* containing either
850 pRAB11: *walR*^{FLAG} / *vraR*^{FLAG} / *hptR*^{FLAG} / *saeR*^{FLAG} or pRAB11^{FLAG} only were grown at 37°C with
851 shaking at 200 rpm. Overnight cultures were diluted 1:100 in fresh LB (100 ml) in a 1 L baffled
852 flask and grown to an OD600nm of 0.5, induced with 100 ng/ml of anhydrotetracycline and
853 grown for a further hour. Cells were crosslinked by direct addition of methanol free
854 formaldehyde (Pierce) to cultures (final concentration of 1% (v/v)) and incubated with gentle
855 mixing (rotating platform) for 15 min at room temperature. The crosslinking reaction was
856 quenched by addition of glycine to a final concentration of 400 mM and incubated a further
857 15 min. Cells were pelleted (7,000xg/10min/4°C), washed three times with ice-cold PBS and
858 the pellet stored at -80°C. For cell lysis, cells were suspended in 1ml of lysis buffer (50 mM
859 Tris-HCl [pH 7.4], 150 mM NaCl, 0.1% Triton X-100, 100 µg / ml lysostaphin (Ambi), 500 µg /
860 ml RNaseA, complete mini protease inhibitor EDTA free containing 100 um zirconium beads)
861 and incubated for 20 min at 37°C. The weakened cells were then disrupted using bead beating
862 (6000 rpm for 1 min; Precellys 24 instrument) and the cell lysate clarified by centrifugation
863 (20,000*xg/*10min/4°C). The cation concentration of the lysate was adjusted with $MgCl_2$ and
864 $CaCl_2$ to 100 mM. The DNA was sheared by the addition of a range of DNase I (NEB)
865 concentrations (0.5 – 2U), in a 200 µL volume, followed by incubation at 37°C for 10 min. The
866 reaction was quenched by the addition of EDTA to 50 mM on ice. The degree of DNA
867 fragmentation was assessed by electrophoresis of samples on a 2% (v/v) agarose TAE gel.
868 Samples showing maximal fragmentation at between 100-300 bp were subjected to
869 immunoprecipitation. Lysis buffer (made up to 4 ml - omitting lysostaphin and RNase A)
870 containing 10 µg of M2-anti FLAG antibody was added and incubated overnight at 4°C on a
871 rotating platform in a 15 ml tube. A 100 µl aliquot of Protein G agarose (Pierce) was added to

872 the lysate and incubated a further 2h at room temperature. The sample was centrifuged
873 (2,500 *xg*/3 min/22°C) and the agarose pellet washed three time with 4 ml of IP buffer (25mM
874 Tris.Cl [pH 7.2], 150mM NaCl) and finally resuspended in 200 µl of elution buffer (10mM Tris.Cl
875 [pH 8], 1mM EDTA, 1% SDS containing 100µg of proteinase K). Crosslinks were reversed
876 incubation for 2h at 37°C and then 9h at 65°C with shaking at 1400 rpm. Finally, eluted DNA
877 was cleaned up by PCR purification (QiaQuick PCR purification kit, Qiagen). DNA libraries were
878 prepared with NEBNext® Ultra™ II DNA Library Prep Kit for Illumina and sequenced using an
879 Illumina MiSeq.

880

881 **ChIP-seq read mapping, peak identification, and motif searching.**

882 MiSeq reads from each of the five experiments (pRAB11: *walR*^{FLAG} / *vraR*^{FLAG} / *hptR*^{FLAG} /
883 *saeR*^{FLAG} or pRAB11^{FLAG} only) were first mapped to the *S. aureus* USA300 NC_007793 reference
884 chromosome using *samtools*. The resulting *.bam* and *.sam* files were used to create tag counts
885 (*i.e.* mapped reads) with the *makeTagDirectory* script within *homer* [93]. The *homer* peak
886 identification tool (*findPeaks*) was extensively explored but high levels of background reads
887 were detected and precluded further use of *homer* for peak detection. An alternative strategy
888 was developed by building read coverage plots for viewing in Artemis [94], using *samtools* and
889 the command *% samtools depth -aa [target_file_name].bam [subtraction_file_name].bam |*
890 *cut -f3,4 | perl -nae 'use List::Util qw(max); print max(0, $F[0]-$F[1]),"\n";' >*
891 *[target_peaks].userplot*. This created a coverage plot of those regions of the *S. aureus* USA300
892 NC_007793 chromosome specifically bound by a given response regulator, relative the
893 response regulator sequence reads in the subtraction set. These subtraction sets were a
894 concatenation of a random selection of 20% of the sequence reads for the three response

895 regulators and the plasmid-only control combined. Thus, for peak discovery of WalR-binding
896 sites, an Artemis userplot was prepared from *vraR*^{FLAG} / *hptR*^{FLAG} / *saeR*^{FLAG} and pRAB11^{FLAG}
897 subtracted from *walR*^{FLAG}**.**The same method was used to generate userplots and discover
898 binding peaks for the remaining three response regulators. The '*create feature from graph*
899 *function*' in *Artemis* was then used to define chromosome regions represented by the
900 subtraction coverage plots. These regions were mapped to the NRS384 genome in Geneious
901 Prime (v2023.03) and searched using TGTNNNNNNNNTGT +/- 5bp as input. Output sequences
902 were combined with motif regions +/- 5bp for the following previously experimentally
903 validated WalR regulon members; SAUSA300_0739, SAUSA300_0955, SAUSA300_2051,
904 SAUSA300_2253, SAUSA300_2503 [13, 27] and input to WebLogo [95]. The resultant sequence logo
905 was converted to IUPAC code and used to search the NRS384 genome using Geneious Prime
906 (v2023.03).

907

908 **Mapping TSS in relation to WalR binding sites**

909 The *S. aureus* NRS384 genome was annotated in Geneious Prime (v2023.03) with predicted
910 transcriptional start sites (TSS) as defined in a previous study [43]. The 500 bp upstream of a
911 predicted TSS were extracted and manually annotated with -35 and -10 elements and
912 predicted WalR binding sites. T-tests (run in Stata v16.0) were used to test associations
913 between WalR binding site position and orientation, with gene expression data from RNA-
914 seq.

915

916 **Essentiality analysis**

917 Essentiality of *S. aureus* genes was called if a locus had been described as essential in two
918 previous studies [96, 97] and did not harbour a transposon insertion in the Nebraska transposon
919 library [98]. Genes were defined as belonging to the core genome if they were present in every
920 strain of the *Aureo*Wiki orthologue table (https://aureowiki.med.uni-
921 greifswald.de/download_orthologue_table)[99]. Data from RNA-seq, ChIP-seq, and the
922 essentiality and core genome analysis was integrated in R (v4.0.3, https://www.r-
923 project.org/) with RStudio 2022.02.0+443 using dplyr (v1.0.8) and tibble (v3.1.6), then
924 visualised using UpSetR (v1.4.0) [98] with ggplot2(v3.3.5).

925

926 **Immunofluorescence microscopy and image analysis**

927 *S. aureus* cells were grown in LB to exponential phase. Bacteria corresponding to an OD_{600nm}
928 of 10 were centrifuged at 4000 x g for 15 min at 4°C and the pellets washed twice with sterile
929 ice-cold PBS. Bacterial pellets were resuspended with paraformaldehyde 4% (Sigma) and fixed
930 for 10 min on ice. Cells are pelleted at 3000 x *g* and washed three time with PBS. Fixed cells
931 were resuspended at a density of 1 unit OD^{600}/ml in PBS. Twenty-five microlitres of fixed *S.*
932 *aureus* cells were applied on round coverslips pre-treated with 0.1% poly-L-lysin (Thermo
933 Fisher Scientific) and allowed to adhere for 20 minutes. Coverslips were washed twice with
934 PBS and incubated with a blocking buffer (PBS-BSA 1% supplemented with normal donkey
935 serum 1:10, Abcam) during 1h. Coverslips were then incubated with primary anti-protein A
936 antibody (Jackson Immunoresearch, chicken IgY) at 1:500 concentration in blocking buffer for
937 2 hours at room temperature. Coverslips were then washed three times with PBS and
938 incubated with 1:1000 secondary antibody (Jackson Immunoresearch, donkey IgG anti-IgY
939 coupled to A647) diluted in blocking buffer for 1h in the dark at room temperature. Coverslips

940 were then washed three times with PBS and incubated with 1:500 BODIPY-Vancomycin FL
941 (Thermo Fisher Scientific) and 1:1000 Hoescht 33342 solution (Sigma) during 15 minutes in
942 the dark. Coverslips are washed twice in PBS and once in distilled water, air-dried and
943 mounted on slides with Prolong platinum (Thermo Fisher Scientific). Imaging was performed
944 using the LSM900 confocal microscope (Carl Zeiss, North Ride). Images were taken using an
945 Airyscan2 SR mode and the raw data was deconvolved using Huygens Deconvolution software
946 (Scientific Volume Imaging b.v., Netherlands). Images were analysed in a semi-automated
947 way using a custom script written with ImageJ macro and FIJI [100]. Briefly, individual bacterial
948 cells were segmented from the channel 488 (BODIPY-Vancomycin) staining using
949 Morphological Segmentation Plugin [82]. The intensity of protein A signal (channel1) was
950 measured from the outline of each *S. aureus* cell and presented as a coefficient of variation
951 (the ratio of the standard deviation to the mean).

952

953 **Growth curves, other phenotypic testing.**

954 For measurement of growth curves, *S. aureus* was grown overnight in BHI broth at 37°C and
955 subsequently diluted into fresh BHI broth to an $OD600_{nm}$ of 0.05. Growth was measured for 8
956 hours at 37°C with 300 rpm dual orbital shaking in a 96 well plate (Corning) using a Clariostar
957 Plus (BMG) plate reader.

958

959 **Antibacterial susceptibility testing**

960 Minimum inhibitory concentrations of antibacterial agents were determined by broth
961 microdilution; bacteria were exposed to 2-fold serial dilutions of antibacterial agents in

962 Mueller-Hinton broth 2 (BBL, BD) according to the guidelines provided by the Clinical and
963 Laboratory Standards Institute . Vancomycin susceptibility was assessed using gradient plates
964 as previously described [101].

965

966 **Lysostaphin sensitivity**

967 An overnight 5ml BHI culture of each strain was diluted 1:100 in an Eppendorf tube containing
968 fresh BHI containing different final concentrations (0 - 1.6 µg / ml) of lysostaphin (Ambi). Cells
969 were then incubated statically for 90 min at 37°C in a water bath with the CFU/ml determined
970 by dilution and spot plating onto BHI agar. Plates were incubated for 18 h at 37°C before
971 enumeration.

972

973 **Heat and Congo red sensitivity**

974 An overnight 5ml BHI culture of each strain was diluted in PBS to 10^{-6} before 5 µl of each
975 dilution was spotted onto either BHI agar (heat) or BHI agar containing 0.1 or 0.25 µg/ml of
976 congo red (Sigma). Plates were incubated for 18 h at 37°C before photography.

977

978 **Flowcytometry analysis**

979 Bacterial cells were grown in LB to exponential phase. One-unit OD600 equivalent of WT,
980 Δ*yycHI* and $WalK_{T389A}$ strains (corresponding to 5 x 10^8 bacterial per ml) were centrifuged at
981 5000*xg* for 5 min, and the bacterial pellet washed three times with sterile PBS. Bacterial cells
982 were fixed with paraformaldehyde 4% (in PBS) for 10 minutes at room temperature (RT) and

983 fixed cells were washed 5 times with PBS. Cells were incubated in blocking buffer (PBS with
984 3% BSA (Sigma), 1:100 FcR-blocker (Miltenyi Biotec) and Tween 0.02%) during 1 hour at RT.

985 Bacterial cells were then incubated with polyclonal antibodies raised in rabbit against whole
986 fixed cells of *S. aureus* USA300 strain JE2::*spa* [98], (1:1000 anti-SA, WEHI antibody technology
987 platform), resuspended in blocking buffer supplemented with normal donkey serum (1:10,
988 Abcam) for two hours on a rotary tube mixer at RT, protected from light. Following incubation,
989 bacterial cells were washed three times with blocking buffer and incubated 45 min protected
990 from light, with secondary antibodies resuspended in blocking buffer with anti-rabbit
991 secondary antibody (donkey anti-rabbit coupled to Alexa 555 fluorophore, 1:2000 dilution,
992 Invitrogen), separately or in combination with SYTO9 (4 mM, Invitrogen).

993 Labelled bacteria were washed three times with blocking buffer, then twice with PBS, and
994 resuspended in a final volume of 500 mL of PBS. Bacterial cells (n: 80,000) were analysed by
995 flow cytometry using the CytoFLEX S and CytExpert software (Beckman and Coulter). Data
996 analysis was performed using FlowJo software (version 10.8.1).

997

998 **LTA extraction, purification, and analysis by PAGE**

999 For extraction and analysis of LTA, 50 ml of LB was inoculated with a single colony of NRS384,
1000 NRS384 Δ*yycHI,* NRS384 *walK*$_{T101A}$, NRS384 *walK*$_{T389A,}$ or RN4220, and grown at 37°C with
1001 vigorous shaking for 18 h. Cells were harvested from 30 ml of saturated culture by
1002 centrifugation of (5000 *x g*, 10 min) and LTA was extracted and analysed by PAGE as described
1003 previously [102].

1004

1005 ***CRISPRi constructs and knockdown analysis.***

1006 To generate pSD1 CRISPRi knockdown constructs for *walR, hla* and *hup,* primers
1007 corresponding to the previously described for *walR* (IM1180/IM1181) and *hla*
1008 (IM1182/IM1183) were synthesised from Zhao *et al* [103]. Knockdown primers for *hup* (targeted
1009 the region overlapping and upstream of the *hup* start codon(IM1559/IM1560)) were designed
1010 with the annealed primer pairs for *walR*, *hla* and *hup* cloned into the SapI site of pSD1 as
1011 described previously [104]. Plasmids were then transformed into NRS384. Overnight cultures
1012 (5ml LB, chloramphenicol 10 µg/ml in 50 ml tubes) were then diluted in fresh media 1:100
1013 containing different concentrations of aTc to induce expression of dCAS9, with the optical
1014 density of the cultures followed.

1015 RNA isolation: RNA was isolated from 1ml of cells (induced with either 0 or 100 ng/ml of aTc)
1016 after 5h of growth, as described above. A 1ug aliquot of total RNA was converted into cDNA
1017 with Superscript IV and random hexamers as described previously [105]. For RT-qPCR, 1 µl of
1018 cDNA was used as template with primers for *gyrB* (IM1020/IM1021), *hla* (IM1026/IM1027),
1019 *walR* (IM1153/IM1154) and *hu* (IM1586/IM1587) with Luna Universal qPCR Master Mix (NEB)
1020 on a Quantstudio 1 PCR machine. The data was normalised to the *gyrB* gene and analysed
1021 with the ΔΔ CT method [106].

1022 Plasmid isolation: Plasmid DNA was isolated from 10 ml of cells at 5h post induction (induced
1023 with 0, 10, 50 and 100 ng/ml aTc). Cells were centrifuged 7,000*xg*/2min pellet was washed in
1024 1ml of PBS and then resuspended in 400 µl of the resuspension buffer (Monarch Miniprep kit
1025 – NEB) containing 50 µg of lysostaphin. The cells were lysed at 37°C for 30 min and then
1026 processed following the kit instructions through one column with elution in 30 µl of elution
1027 buffer. DNA was quantified with the Qubit BR DNA quantification kit and normalised to 15

1028 ng/µl, with the normalised loading (150ng of purified plasmid) assessed on a 1% TAE gel.
1029 Subsequent 1% agarose gels (in 2xTBE) containing 2.5 µg/ml chloroquine were run as
1030 described by Cameron *et al* [107]. Gels (10cm) were run at 10V for 16h which were washed twice
1031 (30 min each wash) in dH_2O and then stained with Sybr Gold for 30 min and subsequently
1032 imaged.

1033 Genomic isolation: Genomic DNA was isolated from the equivalent of OD600nm of 5 after 5h
1034 of growth (induced with 0 or 100 ng/ml aTc). The cell pellet was washed with 1ml of PBS and
1035 resuspended in 90 µl of PBS containing 5 µl of 20 mg/ml RNase A, 50 µg of lysostaphin and
1036 100 µl of the tissue lysis buffer (Monarch Genomic DNA purification kit, NEB). Cells were lysed
1037 at 37°C for 30 min and then processed following the manufactures instructions.

1038 **Analysis of ori-ter ratios**

1039 To measure to ori-ter ratios, genomic DNA prepared after CRISPRi knockdown (as above) was
1040 sequenced using the Illumnia NextSeq (by the Doherty Applied Microbial Genomics facility,
1041 University of Melbourne). Illumina reads were processed and analysed using iRep, as
1042 previously described (v1.1 https://github.com/christophertbrown/iRep [108]).

1043 ***Construction of pSmBIT and pLgBIT split luciferase vectors.***

1044 The vector pRAB11(pC194 replicon) [29] was modified by PCR to restore the consensus *tetO*
1045 upstream of the *tetR* gene (IM1290/IM1291) [109]. As described previously, this reduced the
1046 impact of high level TetR production and allowed leaky expression of the target gene in the
1047 absence of aTc. The above 6.4 kb PCR product was gel extracted, treated with SLiCE and
1048 transformed into *E. coli* IM08B, yielding pRAB11*. To introduce a consensus ribosome binding
1049 site and 8 nt spacer before the start codon (AGGAGGAATTGGAAA) downstream of the two

1050 *tetO* sites (proceeding the gene of interest), pRAB11* was first digested with KpnI and gel
1051 extracted. This was used a template in a PCR (IM513/IM1355), the product digested with KpnI,
1052 gel extracted and ligated. The ligation product was transformed into IM08B yielding
1053 pRAB11*RBS. The *tetR**-RBS fragment was digested from pRAB11*RBS (SphI/KpnI) and
1054 ligated into complementary digested pCN34 (pT181 replicon) [110] yielding pCN34*RBS. Both
1055 pRAB11*RBS and pCN34*RBS were digested with KpnI, gel extracted and used as template in
1056 a PCR (IM515/IM1356). The following combinations were combined with 50 ng of each 1.
1057 pRAB11*RBS PCR and LINKER(GSSGGGGSGGGGSSG)-SmBIT gBlock. 2. pCN34*RBS PCR and
1058 LINKER-LgBIT gBlock. gBlock sequences were codon optimised for *S. aureus* The SLiCE
1059 reactions were transformed into IM08B yielding either pSmBIT or pLgBIT, with both vectors
1060 were fully sequenced to validate.

1061 ***Cloning into split luciferase vectors***

1062 Either pSmBIT and pLgBIT were digested with KpnI, gel extracted and used as template for
1063 PCR with primers IM515/IM1360. The pSmBIT or pLgBIT amplimers were combined with
1064 amplified open reading frames with stop codon removed and tailed with 5'-
1065 GATAGAGTATGATGAGGAGGAATTGGAAA-3' forward or 5'-GAACCACCACCACCACTAGAACC-3'
1066 sequences complementary to the vector.

1067 WalR and WalK alleles were PCR amplified with IM1363/IM1364 and IM1365/IM1366,
1068 respectively, then SLiCE cloned into pSmBIT (for *walR* alleles) or pLgBIT (for *walK* alleles) and
1069 transformed into IM08B. For *S. aureus* transformations, at least 1 µg of pLgBIT(+*walK* allele)
1070 and pSmBIT(+ *walR* allele) were purified from IM08B and co-electroporated into NRS384 with
1071 selection on BHI agar containing 10 ug/ml chloramphenicol and 50 ug/ml kanamycin.

1072 ***Chromosomal tagging of WalR-SmBIT and WalK-LgBIT***

1073 To access the functional interaction of WalR/WalK under native levels of protein of
1074 production, the native copy on the chromosome was tagged with SmBIT for WalR and LgBIT
1075 for WalK. The regions of DNA were assembled as follows. 1. *walR*-SmBIT-*walK*: *walR*-SmBIT
1076 was amplified from pSmBIT-*walR* with IM107/IM1517 and a downstream fragment
1077 encompassing *walK* was amplified with IM1516/IM10 from NRS384 genomic DNA. Both were
1078 gel extracted and joined by SOE-PCR. 2. *walK*-LgBIT-*yycH*: *walK*-LgBIT was amplified from
1079 pLgBIT-*walK* with IM7/IM1519 and a downstream fragment encompassing 500bp of *yycH* was
1080 amplified with IM1518/IM44 on NRS384 genomic DNA. Both were gel extracted and joined
1081 by SOE-PCR. Either amplimer was SLiCE cloned into pIMAY-Z and transformed into IM08B. The
1082 above cloning steps and *S. aureus* allelic exchange was performed as described by Monk and
1083 Stinear [87]. Presence of *walR*-SmBIT and *walK*-LgBIT were screened by colony PCR with
1084 IM1360/IM1368 and IM1360/IM44, respectively. Genomic DNA was isolated from the strains
1085 and whole genome sequenced.

1086

1087 ***Growth and luciferase curves***

1088 An overnight 5 ml LB containing antibiotics (in a 50ml tube) were grown overnight. The culture
1089 was diluted 1:100 in fresh LB supplemented with chloramphenicol and kanamycin including a
1090 1:5000 dilution of the Nano-Glo® Luciferase Assay Substrate (Promega). Preliminary growth
1091 curves in the presence of the substrate showed no impact on growth at this concentration.
1092 The culture was then dispensed in triplicate (200 µl) black/clear bottom 96 well plates (Cat
1093 no. 165305, Themofisher). The plates were sealed with MicroAmp™ Optical Adhesive Film
1094 (Thermofisher) and incubated at 37°C with dual orbital shaking at 300 rpm (Clariostar Plus,

1095 BMG). Every 10 minutes the plate was read at OD600nm and light emission (1s exposure)
1096 collected over a 8 h period.

1097 ***Bacterial luciferase reporter plasmid***

1098 To construct pIMK1-LUX, the Listeria phage integrase vector pIMK was digested with
1099 SphI/BglII to excise the PSA integrase and replace it with the PCR amplified (IM1241/IM1242)
1100 low copy number pSK41 replicon from pLOW, yielding pIMK1. Vectors pIMK1 and pPL2*lux*
1101 were then digested with SalI/PstI and the gel extracted pIMK1 backbone ligated to the
1102 bacterial luciferase operon from pPL2*lux*. The vector pIMK1-LUX produces exact promoter
1103 fusions which can be cloned into the SalI/SwaI digested vector, as described previously [111].
1104 Promoters for *walR* (IM1222/IM32), *sasD* (IM1216/IM248 (Wt) or IM1217(ccc)), *sle1*
1105 (IM1295/IM1115; IM1114/IM1296), *0602* (IM1294/IM1119; IM1118/IM1062), *ltaS*
1106 (IM1218/IM1117; IM1116/IM1219), $ssaA^{CCCII}$ (IM1297/IM1121; IM1120/IM1298), $isaA^{CCCI}$
1107 (IM1220/IM1123; IM1122/IM1221), $isaA^{CCCII}$ (IM1220/IM1125; IM1124/IM1221), *tarF*
1108 (LS451/LS448; LS449/LS452), *tagG* (LS457/LS454; LS455/LS458), *dnaA* (IM1745/IM1744;
1109 IM1743/IM1746), $dnaD^{CCCI}$ (LS471/LS466; LS467/LS472), $dnaD^{CCCII}$ (LS471/LS468;
1110 LS469/LS472,) *rplK* (IM1734/LS143; LS144/IM1735), *hup* (IM1289/IM1290; IM1291/IM1292),
1111 $dnaA^{CCCI}$ (LS443/LS440; LS441/IM1746), $dnaA^{CCCII}$ (LS443/LS438; LS439/IM1746), $dnaA^{CCCIII}$
1112 (LS443/IM1743; IM1744/IM1746), and *prs* (IM1285/LS139; IM140/IM1288) were PCR
1113 amplified from genomic DNA with either the outer set (Wt promoter) or SOE-PCR with the
1114 four primers (ccc promoter). The amplimers were digested with SalI, gel extracted and cloned
1115 into the above double digested vector. Plasmids isolated from IM08B were transformed into
1116 NRS384 Wt. An overnight 5ml LB culture with kanamycin was diluted 1:100 in fresh LB

1117 containing kanamycin with growth curves and light emission measured as described above
1118 for the split luciferase with the substrate omitted.

1119 **Data visualisation**

1120 Graphs were generated in R (v4.0.3, https://www.r-project.org/)or GraphPad Prism (v9.3.1)
1121 software packages.

1122 **Data availability:** The DNA sequence reads for ChIP-seq and RNA-seq have been submitted to
1123 the NCBI Gene Expression Omnibus (GEO) repository under accession number GSE212321.
1124 DNA sequence reads for ori-ter analysis have been submitted to NCBI under Bioproject ID
1125 PRJNA886746.

1126 **Acknowledgements**

1127 We are grateful to the following colleagues of for their advice, assistance, and input into this work:
1128 Justin Clarke, Charlie Higgs, Danielle Ingle, Karinna Saxby. T.P.S. is supported by NHMRC Research
1129 Gramt (APP1105525) and NHMRC project grant GNT1145075. H. E. G. M. is supported through an
1130 NHMRC ideas grant 2003192. A.M.T. is supported by an Australian Government Research Training
1131 Program scholarship.

1132

1133

1134 ## References

1135 1. Care ACoSaQiH. AURA 2021: Fourth Australian report on antimicrobial use and resistance in
1136 human health. (2021).

1137
1138 2. Howden BP, Peleg AY, Stinear TP. The evolution of vancomycin intermediate Staphylococcus
1139 aureus (VISA) and heterogenous-VISA. *Infect Genet Evol* **21**, 575-582 (2014).

1140
1141 3. Tong SY, Davis JS, Eichenberger E, Holland TL, Fowler VG, Jr. Staphylococcus aureus
1142 infections: epidemiology, pathophysiology, clinical manifestations, and management. *Clin*
1143 *Microbiol Rev* **28**, 603-661 (2015).

1144
1145 4. Bai AD*, et al.* Staphylococcus aureus bacteraemia mortality: a systematic review and meta-
1146 analysis. *Clin Microbiol Infect* **28**, 1076-1084 (2022).

1147
1148 5. Wozniak TM, Dyda A, Merlo G, Hall L. Disease burden, associated mortality and economic
1149 impact of antimicrobial resistant infections in Australia. *Lancet Reg Health West Pac* **27**,
1150 100521 (2022).

1151
1152 6. Martin PK, Li T, Sun D, Biek DP, Schmid MB. Role in cell permeability of an essential two-
1153 component system in Staphylococcus aureus. *J Bacteriol* **181**, 3666-3673 (1999).

1154
1155 7. Delaune A, Poupel O, Mallet A, Coic YM, Msadek T, Dubrac S. Peptidoglycan crosslinking
1156 relaxation plays an important role in Staphylococcus aureus WalKR-dependent cell viability.
1157 *PLoS One* **6**, e17054 (2011).

1158
1159 8. Dubrac S, Msadek T. Identification of genes controlled by the essential YycG/YycF two-
1160 component system of Staphylococcus aureus. *J Bacteriol* **186**, 1175-1181 (2004).

1161
1162 9. Villanueva M*, et al.* Sensory deprivation in Staphylococcus aureus. *Nat Commun* **9**, 523
1163 (2018).

1164
1165 10. Fabret C, Hoch JA. A two-component signal transduction system essential for growth of
1166 Bacillus subtilis: implications for anti-infective therapy. *J Bacteriol* **180**, 6375-6383 (1998).

1167
1168 11. Dubrac S, Msadek T. Tearing down the wall: peptidoglycan metabolism and the WalK/WalR
1169 (YycG/YycF) essential two-component system. *Adv Exp Med Biol* **631**, 214-228 (2008).

1170
1171 12. Howell A*, et al.* Genes controlled by the essential YycG/YycF two-component system of
1172 Bacillus subtilis revealed through a novel hybrid regulator approach. *Mol Microbiol* **49**, 1639-
1173 1655 (2003).

1174

1175 13. Dubrac S, Boneca IG, Poupel O, Msadek T. New insights into the WalK/WalR (YycG/YycF)
1176 essential signal transduction pathway reveal a major role in controlling cell wall metabolism
1177 and biofilm formation in Staphylococcus aureus. *J Bacteriol* **189**, 8257-8269 (2007).

1178
1179 14. Bisicchia P*, et al.* The essential YycFG two-component system controls cell wall metabolism
1180 in Bacillus subtilis. *Mol Microbiol* **65**, 180-200 (2007).

1181
1182 15. Noone D, Howell A, Collery R, Devine KM. YkdA and YvtA, HtrA-like serine proteases in
1183 Bacillus subtilis, engage in negative autoregulation and reciprocal cross-regulation of ykdA
1184 and yvtA gene expression. *J Bacteriol* **183**, 654-663 (2001).

1185
1186 16. Dubrac S, Bisicchia P, Devine KM, Msadek T. A matter of life and death: cell wall homeostasis
1187 and the WalKR (YycGF) essential signal transduction pathway. *Mol Microbiol* **70**, 1307-1322
1188 (2008).

1189
1190 17. Cameron DR, Jiang JH, Kostoulias X, Foxwell DJ, Peleg AY. Vancomycin susceptibility in
1191 methicillin-resistant Staphylococcus aureus is mediated by YycHI activation of the WalRK
1192 essential two-component regulatory system. *Sci Rep* **6**, 30823 (2016).

1193
1194 18. Szurmant H, Mohan MA, Imus PM, Hoch JA. YycH and YycI interact to regulate the essential
1195 YycFG two-component system in Bacillus subtilis. *J Bacteriol* **189**, 3280-3289 (2007).

1196
1197 19. Fukuchi K, Kasahara Y, Asai K, Kobayashi K, Moriya S, Ogasawara N. The essential two-
1198 component regulatory system encoded by yycF and yycG modulates expression of the ftsAZ
1199 operon in Bacillus subtilis. *Microbiology (Reading)* **146 (Pt 7)**, 1573-1583 (2000).

1200
1201 20. Fukushima T, Furihata I, Emmins R, Daniel RA, Hoch JA, Szurmant H. A role for the essential
1202 YycG sensor histidine kinase in sensing cell division. *Mol Microbiol* **79**, 503-522 (2011).

1203
1204 21. Fukushima T, Szurmant H, Kim EJ, Perego M, Hoch JA. A sensor histidine kinase co-ordinates
1205 cell wall architecture with cell division in Bacillus subtilis. *Mol Microbiol* **69**, 621-632 (2008).

1206
1207 22. Takada H*, et al.* Essentiality of WalRK for growth in Bacillus subtilis and its role during heat
1208 stress. *Microbiology (Reading)* **164**, 670-684 (2018).

1209
1210 23. Poupel O*, et al.* Transcriptional Analysis and Subcellular Protein Localization Reveal Specific
1211 Features of the Essential WalKR System in Staphylococcus aureus. *PLoS One* **11**, e0151449
1212 (2016).

1213
1214 24. Ng WL, Robertson GT, Kazmierczak KM, Zhao J, Gilmour R, Winkler ME. Constitutive
1215 expression of PcsB suppresses the requirement for the essential VicR (YycF) response
1216 regulator in Streptococcus pneumoniae R6. *Mol Microbiol* **50**, 1647-1663 (2003).

1217

1218 25. Dobihal GS, Brunet YR, Flores-Kim J, Rudner DZ. Homeostatic control of cell wall hydrolysis
1219 by the WalRK two-component signaling pathway in Bacillus subtilis. *Elife* **8**, (2019).

1220
1221 26. Monk IR*, et al.* Zinc-binding to the cytoplasmic PAS domain regulates the essential WalK
1222 histidine kinase of Staphylococcus aureus. *Nat Commun* **10**, 3067 (2019).

1223
1224 27. Delauné A*, et al.* The WalKR system controls major staphylococcal virulence genes and is
1225 involved in triggering the host inflammatory response. *Infect Immun* **80**, 3438-3453 (2012).

1226
1227 28. Rapun-Araiz B*, et al.* Systematic Reconstruction of the Complete Two-Component Sensorial
1228 Network in Staphylococcus aureus. *mSystems* **5**, (2020).

1229
1230 29. Helle L*, et al.* Vectors for improved Tet repressor-dependent gradual gene induction or
1231 silencing in Staphylococcus aureus. *Microbiology (Reading)* **157**, 3314-3323 (2011).

1232
1233 30. Belcheva A, Verma V, Golemi-Kotra D. DNA-binding activity of the vancomycin resistance
1234 associated regulator protein VraR and the role of phosphorylation in transcriptional
1235 regulation of the vraSR operon. *Biochemistry* **48**, 5592-5601 (2009).

1236
1237 31. Sun F, Li C, Jeong D, Sohn C, He C, Bae T. In the Staphylococcus aureus two-component
1238 system sae, the response regulator SaeR binds to a direct repeat sequence and DNA binding
1239 requires phosphorylation by the sensor kinase SaeS. *J Bacteriol* **192**, 2111-2127 (2010).

1240
1241 32. Yang Y, Sun H, Liu X, Wang M, Xue T, Sun B. Regulatory mechanism of the three-component
1242 system HptRSA in glucose-6-phosphate uptake in Staphylococcus aureus. *Med Microbiol*
1243 *Immunol* **205**, 241-253 (2016).

1244
1245 33. Gründling A, Schneewind O. Synthesis of glycerol phosphate lipoteichoic acid in
1246 Staphylococcus aureus. *Proc Natl Acad Sci U S A* **104**, 8478-8483 (2007).

1247
1248 34. Libby EA, Goss LA, Dworkin J. The Eukaryotic-Like Ser/Thr Kinase PrkC Regulates the Essential
1249 WalRK Two-Component System in Bacillus subtilis. *PLoS Genet* **11**, e1005275 (2015).

1250
1251 35. Huynh TN, Noriega CE, Stewart V. Conserved mechanism for sensor phosphatase control of
1252 two-component signaling revealed in the nitrate sensor NarX. *Proc Natl Acad Sci U S A* **107**,
1253 21140-21145 (2010).

1254
1255 36. Monk IR*, et al.* Zinc-binding to the cytoplasmic PAS domain regulates the essential WalK
1256 histidine kinase of Staphylococcus aureus. *Nature Communications* **10**, 3067 (2019).

1257
1258 37. Martin PK*, et al.* Novel locus required for expression of high-level macrolide-lincosamide-
1259 streptogramin B resistance in Staphylococcus aureus. *J Bacteriol* **184**, 5810-5813 (2002).

1260

1261 38. Buschiazzo A, Trajtenberg F. Two-Component Sensing and Regulation: How Do Histidine
1262 Kinases Talk with Response Regulators at the Molecular Level? *Annu Rev Microbiol* **73**, 507-
1263 528 (2019).

1264
1265 39. Brown M, Hall A, Zahn H, Eisenberg M, Erickson S. Bacteriophage-Based Detection of
1266 Staphylococcus aureus in Human Serum. *Viruses* **14**, (2022).

1267
1268 40. Hu J, Zhang X, Liu X, Chen C, Sun B. Mechanism of reduced vancomycin susceptibility
1269 conferred by walK mutation in community-acquired methicillin-resistant Staphylococcus
1270 aureus strain MW2. *Antimicrob Agents Chemother* **59**, 1352-1355 (2015).

1271
1272 41. DeDent AC, McAdow M, Schneewind O. Distribution of protein A on the surface of
1273 Staphylococcus aureus. *J Bacteriol* **189**, 4473-4484 (2007).

1274
1275 42. Heilmann C, Hussain M, Peters G, Götz F. Evidence for autolysin-mediated primary
1276 attachment of Staphylococcus epidermidis to a polystyrene surface. *Mol Microbiol* **24**, 1013-
1277 1024 (1997).

1278
1279 43. Prados J, Linder P, Redder P. TSS-EMOTE, a refined protocol for a more complete and less
1280 biased global mapping of transcription start sites in bacterial pathogens. *BMC Genomics* **17**,
1281 849 (2016).

1282
1283 44. Hardt P*, et al.* The cell wall precursor lipid II acts as a molecular signal for the Ser/Thr kinase
1284 PknB of Staphylococcus aureus. *International Journal of Medical Microbiology* **307**, 1-10
1285 (2017).

1286
1287 45. Sengupta M, Jain V, Wilkinson BJ, Jayaswal RK. Chromatin immunoprecipitation identifies
1288 genes under direct VraSR regulation in Staphylococcus aureus. *Can J Microbiol* **58**, 703-708
1289 (2012).

1290
1291 46. Martin E*, et al.* DNA replication initiation in Bacillus subtilis: structural and functional
1292 characterization of the essential DnaA–DnaD interaction. *Nucleic Acids Research* **47**, 2101-
1293 2112 (2018).

1294
1295 47. Huang YH, Lien Y, Huang CC, Huang CY. Characterization of Staphylococcus aureus
1296 Primosomal DnaD Protein: Highly Conserved C-Terminal Region Is Crucial for ssDNA and PriA
1297 Helicase Binding but Not for DnaA Protein-Binding and Self-Tetramerization. *PLoS One* **11**,
1298 e0157593 (2016).

1299
1300 48. Buchad H, Nair M. The small RNA SprX regulates the autolysin regulator WalR in
1301 Staphylococcus aureus. *Microbiological Research* **250**, 126785 (2021).

1302
1303 49. Pang T, Wang X, Lim HC, Bernhardt TG, Rudner DZ. The nucleoid occlusion factor Noc
1304 controls DNA replication initiation in Staphylococcus aureus. *PLoS Genet* **13**, e1006908
1305 (2017).

1306
1307 50. Percy MG, Gründling A. Lipoteichoic acid synthesis and function in gram-positive bacteria.
1308 *Annu Rev Microbiol* **68**, 81-100 (2014).

1309
1310 51. Kho K, Meredith TC. Salt-Induced Stress Stimulates a Lipoteichoic Acid-Specific Three-
1311 Component Glycosylation System in Staphylococcus aureus. *J Bacteriol* **200**, (2018).

1312
1313 52. Vickery CR, Wood BM, Morris HG, Losick R, Walker S. Reconstitution of Staphylococcus
1314 aureus Lipoteichoic Acid Synthase Activity Identifies Congo Red as a Selective Inhibitor. *J Am*
1315 *Chem Soc* **140**, 876-879 (2018).

1316
1317 53. O'Neill AJ, Chopra I. Preclinical evaluation of novel antibacterial agents by microbiological
1318 and molecular techniques. *Expert Opin Investig Drugs* **13**, 1045-1063 (2004).

1319
1320 54. Kim DH*, et al.* β-Arm flexibility of HU from Staphylococcus aureus dictates the DNA-binding
1321 and recognition mechanism. *Acta Crystallogr D Biol Crystallogr* **70**, 3273-3289 (2014).

1322
1323 55. Stojkova P, Spidlova P, Stulik J. Nucleoid-Associated Protein HU: A Lilliputian in Gene
1324 Regulation of Bacterial Virulence. *Front Cell Infect Microbiol* **9**, 159 (2019).

1325
1326 56. Rouvière-Yaniv J, Yaniv M, Germond J-E. E. coli DNA binding protein HU forms nucleosome-
1327 like structure with circular double-stranded DNA. *Cell* **17**, 265-274 (1979).

1328
1329 57. Karaboja X, Wang X. HBsu Is Required for the Initiation of DNA Replication in Bacillus subtilis.
1330 *J Bacteriol*, e0011922 (2022).

1331
1332 58. Karaboja X, Wang X. HBsu Is Required for the Initiation of DNA Replication in Bacillus subtilis.
1333 *J Bacteriol* **204**, e0011922 (2022).

1334
1335 59. Hancock LE, Perego M. Systematic inactivation and phenotypic characterization of two-
1336 component signal transduction systems of Enterococcus faecalis V583. *J Bacteriol* **186**, 7951-
1337 7958 (2004).

1338
1339 60. Kallipolitis BH, Ingmer H. Listeria monocytogenes response regulators important for stress
1340 tolerance and pathogenesis. *FEMS Microbiol Lett* **204**, 111-115 (2001).

1341
1342 61. Müh U, Ellermeier CD, Weiss DS. The WalRK Two-Component System Is Essential for Proper
1343 Cell Envelope Biogenesis in Clostridioides difficile. *J Bacteriol* **204**, e0012122 (2022).

1344
1345 62. Wagner C*, et al.* Genetic analysis and functional characterization of the Streptococcus
1346 pneumoniae vic operon. *Infect Immun* **70**, 6121-6128 (2002).

1347

1348 63. Howden BP*, et al.* Evolution of multidrug resistance during Staphylococcus aureus infection
1349 involves mutation of the essential two component regulator WalKR. *PLoS Pathog* **7**,
1350 e1002359 (2011).

1351
1352 64. Wörmann ME, Reichmann NT, Malone CL, Horswill AR, Gründling A. Proteolytic cleavage
1353 inactivates the Staphylococcus aureus lipoteichoic acid synthase. *J Bacteriol* **193**, 5279-5291
1354 (2011).

1355
1356 65. Kuroda M, Kuroda H, Oshima T, Takeuchi F, Mori H, Hiramatsu K. Two-component system
1357 VraSR positively modulates the regulation of cell-wall biosynthesis pathway in
1358 Staphylococcus aureus. *Mol Microbiol* **49**, 807-821 (2003).

1359
1360 66. Belcheva A, Golemi-Kotra D. A close-up view of the VraSR two-component system. A
1361 mediator of Staphylococcus aureus response to cell wall damage. *J Biol Chem* **283**, 12354-
1362 12364 (2008).

1363
1364 67. Fernandes PB, Reed P, Monteiro JM, Pinho MG. Revisiting the Role of VraTSR in
1365 Staphylococcus aureus Response to Cell Wall-Targeting Antibiotics. *J Bacteriol* **204**,
1366 e0016222 (2022).

1367
1368 68. Hancock IC. Bacterial cell surface carbohydrates: structure and assembly. *Biochem Soc Trans*
1369 **25**, 183-187 (1997).

1370
1371 69. Hesser AR, Schaefer K, Lee W, Walker S. Lipoteichoic acid polymer length is determined by
1372 competition between free starter units. *Proc Natl Acad Sci U S A* **117**, 29669-29676 (2020).

1373
1374 70. Fait A*, et al.* Adaptive laboratory evolution and independent component analysis disentangle
1375 complex vancomycin adaptation trajectories. *Proc Natl Acad Sci U S A* **119**, e2118262119
1376 (2022).

1377
1378 71. Lamichhane-Khadka R*, et al.* Apt (Adenine Phosphoribosyltransferase) Mutation in
1379 Laboratory-Selected Vancomycin-Intermediate Staphylococcus aureus. *Antibiotics (Basel)* **10**,
1380 (2021).

1381
1382 72. Barbuti MD, Myrbråten IS, Morales Angeles D, Kjos M. The cell cycle of Staphylococcus
1383 aureus: An updated review. *MicrobiologyOpen* **12**, e1338 (2023).

1384
1385 73. Gallay C*, et al.* CcrZ is a pneumococcal spatiotemporal cell cycle regulator that interacts with
1386 FtsZ and controls DNA replication by modulating the activity of DnaA. *Nature Microbiology* **6**,
1387 1175-1187 (2021).

1388
1389 74. Karaboja X, Wang X. HBsu Is Required for the Initiation of DNA Replication in Bacillus subtilis.
1390 *J Bacteriol* **204**, e00119-00122 (2022).

1391

1392 75. Verma SC, Harned A, Narayan K, Adhya S. Non-specific and specific DNA binding modes of
1393 bacterial histone, HU, separately regulate distinct physiological processes through different
1394 mechanisms. *Mol Microbiol*, (2023).

1395
1396 76. Ohniwa RL, Ushijima Y, Saito S, Morikawa K. Proteomic analyses of nucleoid-associated
1397 proteins in Escherichia coli, Pseudomonas aeruginosa, Bacillus subtilis, and Staphylococcus
1398 aureus. *PLoS One* **6**, e19172 (2011).

1399
1400 77. Gupta M*, et al.* HupB, a nucleoid-associated protein of Mycobacterium tuberculosis, is
1401 modified by serine/threonine protein kinases in vivo. *J Bacteriol* **196**, 2646-2657 (2014).

1402
1403 78. Burnside K*, et al.* Regulation of hemolysin expression and virulence of Staphylococcus aureus
1404 by a serine/threonine kinase and phosphatase. *PLoS One* **5**, e11071 (2010).

1405
1406 79. Takada H, Yoshikawa H. Essentiality and function of WalK/WalR two-component system: the
1407 past, present, and future of research. *Biosci Biotechnol Biochem* **82**, 741-751 (2018).

1408
1409 80. Shah IM, Dworkin J. Induction and regulation of a secreted peptidoglycan hydrolase by a
1410 membrane Ser/Thr kinase that detects muropeptides. *Mol Microbiol* **75**, 1232-1243 (2010).

1411
1412 81. Tiwari S*, et al.* Two-Component Signal Transduction Systems of Pathogenic Bacteria As
1413 Targets for Antimicrobial Therapy: An Overview. *Frontiers in Microbiology* **8**, (2017).

1414
1415 82. Legland D, Arganda-Carreras I, Andrey P. MorphoLibJ: integrated library and plugins for
1416 mathematical morphology with ImageJ. *Bioinformatics* **32**, 3532-3534 (2016).

1417
1418 83. Laws M, Shaaban A, Rahman KM. Antibiotic resistance breakers: current approaches and
1419 future directions. *FEMS Microbiology Reviews* **43**, 490-516 (2019).

1420
1421 84. Tan S, Cho K, Nodwell JR. A defect in cell wall recycling confers antibiotic resistance and
1422 sensitivity in Staphylococcus aureus. *J Biol Chem* **298**, 102473 (2022).

1423
1424 85. Campbell J*, et al.* Synthetic lethal compound combinations reveal a fundamental connection
1425 between wall teichoic acid and peptidoglycan biosyntheses in Staphylococcus aureus. *ACS*
1426 *Chem Biol* **6**, 106-116 (2011).

1427
1428 86. Bilyk BL, Panchal VV, Tinajero-Trejo M, Hobbs JK, Foster SJ. An Interplay of Multiple Positive
1429 and Negative Factors Governs Methicillin Resistance in Staphylococcus aureus. *Microbiol*
1430 *Mol Biol Rev* **86**, e0015921 (2022).

1431
1432 87. Monk IR, Stinear TP. From cloning to mutant in 5 days: rapid allelic exchange in
1433 Staphylococcus aureus. *Access Microbiol* **3**, 000193 (2021).

1434

1435 88. Monk IR, Tree JJ, Howden BP, Stinear TP, Foster TJ. Complete Bypass of Restriction Systems
1436 for Major Staphylococcus aureus Lineages. *mBio* **6**, e00308-00315 (2015).

1437
1438 89. Studier FW. Protein production by auto-induction in high density shaking cultures. *Protein*
1439 *Expr Purif* **41**, 207-234 (2005).

1440
1441 90. Hsieh YW, Alqadah A, Chuang CF. An Optimized Protocol for Electrophoretic Mobility Shift
1442 Assay Using Infrared Fluorescent Dye-labeled Oligonucleotides. *J Vis Exp*, (2016).

1443
1444 91. Bray NL, Pimentel H, Melsted P, Pachter L. Near-optimal probabilistic RNA-seq
1445 quantification. *Nature Biotechnology* **34**, 525-527 (2016).

1446
1447 92. Law CW, Chen Y, Shi W, Smyth GK. voom: Precision weights unlock linear model analysis
1448 tools for RNA-seq read counts. *Genome Biol* **15**, R29 (2014).

1449
1450 93. Duttke SH, Chang MW, Heinz S, Benner C. Identification and dynamic quantification of
1451 regulatory elements using total RNA. *Genome Res* **29**, 1836-1846 (2019).

1452
1453 94. Carver T, Harris SR, Berriman M, Parkhill J, McQuillan JA. Artemis: an integrated platform for
1454 visualization and analysis of high-throughput sequence-based experimental data.
1455 *Bioinformatics* **28**, 464-469 (2012).

1456
1457 95. Crooks GE, Hon G, Chandonia JM, Brenner SE. WebLogo: a sequence logo generator.
1458 *Genome Res* **14**, 1188-1190 (2004).

1459
1460 96. Valentino MD*, et al.* Genes contributing to Staphylococcus aureus fitness in abscess- and
1461 infection-related ecologies. *mBio* **5**, e01729-01714 (2014).

1462
1463 97. Chaudhuri RR*, et al.* Comprehensive identification of essential Staphylococcus aureus genes
1464 using Transposon-Mediated Differential Hybridisation (TMDH). *BMC Genomics* **10**, 291
1465 (2009).

1466
1467 98. Fey PD*, et al.* A genetic resource for rapid and comprehensive phenotype screening of
1468 nonessential Staphylococcus aureus genes. *mBio* **4**, e00537-00512 (2013).

1469
1470 99. Fuchs S*, et al.* AureoWiki-The repository of the Staphylococcus aureus research and
1471 annotation community. *Int J Med Microbiol* **308**, 558-568 (2018).

1472
1473 100. Schindelin J*, et al.* Fiji: an open-source platform for biological-image analysis. *Nat Methods* **9**,
1474 676-682 (2012).

1475
1476 101. Lee JYH*, et al.* Global spread of three multidrug-resistant lineages of Staphylococcus
1477 epidermidis. *Nat Microbiol* **3**, 1175-1185 (2018).

1478
1479 102. Kho K, Meredith TC. Extraction and Analysis of Bacterial Teichoic Acids. *Bio-protocol* **8**, e3078
1480 (2018).

1481
1482 103. Zhao C, Shu X, Sun B. Construction of a Gene Knockdown System Based on Catalytically
1483 Inactive (“Dead”) Cas9 (dCas9) in Staphylococcus aureus. *Applied and*
1484 *Environmental Microbiology* **83**, e00291-00217 (2017).

1485
1486 104. Pryor JM, Potapov V, Kucera RB, Bilotti K, Cantor EJ, Lohman GJS. Enabling one-pot Golden
1487 Gate assemblies of unprecedented complexity using data-optimized assembly design. *PLOS*
1488 *ONE* **15**, e0238592 (2020).

1489
1490 105. Wong Fok Lung T*, et al.* Staphylococcus aureus small colony variants impair host immunity
1491 by activating host cell glycolysis and inducing necroptosis. *Nat Microbiol* **5**, 141-153 (2020).

1492
1493 106. Livak KJ, Schmittgen TD. Analysis of relative gene expression data using real-time
1494 quantitative PCR and the 2(-Delta Delta C(T)) Method. *Methods* **25**, 402-408 (2001).

1495
1496 107. Cameron ADS, Stoebel DM, Dorman CJ. DNA supercoiling is differentially regulated by
1497 environmental factors and FIS in Escherichia coli and Salmonella enterica. *Molecular*
1498 *Microbiology* **80**, 85-101 (2011).

1499
1500 108. Brown CT, Olm MR, Thomas BC, Banfield JF. Measurement of bacterial replication rates in
1501 microbial communities. *Nat Biotechnol* **34**, 1256-1263 (2016).

1502
1503 109. Schleimer N*, et al.* Adaption of an Episomal Antisense Silencing Approach for Investigation of
1504 the Phenotype Switch of Staphylococcus aureus Small-Colony Variants. *Front Microbiol* **10**,
1505 2044 (2019).

1506
1507 110. Charpentier E, Anton AI, Barry P, Alfonso B, Fang Y, Novick RP. Novel cassette-based shuttle
1508 vector system for gram-positive bacteria. *Appl Environ Microbiol* **70**, 6076-6085 (2004).

1509
1510 111. Bron PA, Monk IR, Corr SC, Hill C, Gahan CG. Novel luciferase reporter system for in vitro and
1511 organ-specific monitoring of differential gene expression in Listeria monocytogenes. *Appl*
1512 *Environ Microbiol* **72**, 2876-2884 (2006).

1513

1514

1515